frontiers | Frontiers in Physics

TYPE Review
PUBLISHED 12 October 2022
DOI 10.3389/fphy.2022.898833

OPEN ACCESS

EDITED BY
Mauro Menichelli,
Istituto Nazionale di Fisica Nucleare di Perugia, Italy

REVIEWED BY
Giovanni Verzellesi,
University of Modena and Reggio Emilia, Italy
Francesco Moscatelli,
National Research Council (CNR), Italy

*CORRESPONDENCE
Marzio De Napoli,
marzio.denapoli@ct.infn.it

SPECIALTY SECTION
This article was submitted to Radiation Detectors and Imaging, a section of the journal Frontiers in Physics

RECEIVED 17 March 2022
ACCEPTED 26 July 2022
PUBLISHED 12 October 2022

CITATION
De Napoli M (2022), SiC detectors: A review on the use of silicon carbide as radiation detection material.
Front. Phys. 10:898833.
doi: 10.3389/fphy.2022.898833

SiC detectors: A review on the use of silicon carbide as radiation detection material

Marzio De Napoli*

Istituto Nazionale di Fisica Nucleare (INFN), Sezione di Catania, Catania, Italy

Silicon Carbide (SiC) is a wide bandgap semiconductor with many excellent properties that make it one of the most promising and well-studied materials for radiation particle detection. This review provides an overview of the main advantages in the use of SiC detectors and the current state of research in this field. Key aspects related to material properties, growth techniques, doping, defects, electrical contacts, and characterization methods are summarized, with particular emphasis on how these can be related to detector performance. The most recent and significant experimental results on the use of SiC diodes for the detection of electrons, protons, alpha, ions, UV radiation, x/γ-rays, and neutrons are discussed. The effects of high temperature operation and radiation damage on detector performance are outlined.

KEYWORDS

wide-bandgap semiconductors, silicon carbide (SiC), semiconductor radiation detectors, SiC detector fabrication, SiC detector characterization methods, defects in silicon carbide, radiation detection and measurement, radiation damage

1 Introduction

Silicon Carbide (SiC) is a semiconductor composed of 50% silicon (Si) and 50% carbon (C). The first synthesis of a silicon-carbon composite is reported by Berzelius [1]. SiC is rare in nature; its discovery as a natural mineral, named moissanite after its discoverer, dates back to 1905. SiC as a radiation detector has been demonstrated in as early as the 1960s [2]. However, it was not until the late 1990s that improvements in SiC diode fabrication and material quality led to the first doped SiC epitaxial layers of reasonable quality and renewed interest in this material (for a summary of the history of SiC synthesis, the reader is referred to [3] and references therein). As a result, there was a tremendous acceleration of work investigating the performance of SiC detectors for various types of radiation in the first decade of the new millennium. Progress in SiC detector fabrication continues today, and with it the diffuse interest of researchers around the World in evaluating the performance of SiC detectors of increasingly good quality. There are many reviews on the subject of Silicon Carbide as a radiation detector material, such as those by [4–8], and Capan in 2022 [9]. The idea behind this review is to give readers as complete and up-to-date a summary as possible on SiC radiation detectors. The subject is undoubtedly huge and cannot be covered in detail in a review paper, and that is not the scope. Rather, the goal of this work is to present the basic concepts and results of

the field in a manner that is simultaneously introductory for some aspects and advanced for others. In addition, this review can serve as repository where the reader who wishes to deepen his or her knowledge on a particular topic can refer to the cited references. For this reason, I have tried to include as many references as possible, even though not all of them can be accommodated in a single article.

The overview is organized as follows. Section 2 reviews the electrical and physical properties of silicon carbide relevant to its use as a radiation detector.

Section 3 summarizes the basic concepts behind the structure of a SiC detector and the fabrication techniques of its various parts.

Section 4 reviews the performance of SiC-based devices as radiation detectors for different types of radiation. Here, an attempt is made to give a summary of the main results for each type of radiation, and to mention some of the most important (at least in my personal opinion) results from the various published papers. I have tried to include as many papers as possible, but I apologize in advance for not citing all the interesting papers that have been published on this topic. For most of the cited papers, I have tried to summarize what I think is interesting information that helps focus typical aspects of the field (e.g., a detector structure, typical detector dimensions, doping concentrations, *etc.*) and that helps to understand the reported results.

Finally, the issue of radiation damage in SiC detectors is addressed in a separate section (Section 5), dividing the reported experimental results by the type of radiation used to irradiate the detectors.

2 Physical and electrical properties of SiC

The basic cell of SiC consists of one Si atom with 4 C neighbors and vice versa, forming a tetrahedral structure. This unit is common to all SiC polytypes, which differ from each other by variations in stacking order. The more than 200 crystal polymorphs can be classified by lattice symmetry as cubic (C), hexagonal (H), and rhombohedral (R). The number given before the symmetry letter indicates the number of layers in the stacking sequence, as in 4H-SiC. The different polytypes can be characterized by their hexagonality fraction *fH*, where 2H (3C) has $fH = 1$ ($fH = 0$). The other polytypes consist of lattices with different sequences of hexagonal and cubic stacking layers and can be listed in order of increasing hexagonal packing: 3C, 8H, 6H, 4H, 2H.

The stability of politypes depends on temperature and thus affects the ability to grow large ingots. As a result, the most common and commercially available polytipes are 3C-SiC, 4H-SiC, and 6H-SiC [3].

Table 1 reports some properties of the SiC material compared to Si, diamond (its direct competitor in many areas of radiation detection), and the other wide bandgap semiconductor GaN. Some of the reported values make SiC a very interesting material compared to Si and diamond. Figure 1 highlights the SiC most interesting properties compared to Si and Diamond in connection with its use as a radiation detector material.

A brief description of some of the most important properties of this material, especially with respect to its use as a radiation detector, is given below. For an overview of this topic, see [3].

2.1 Thermal conductivity

Thanks to their high thermal conductivity, detectors based on 4H-SiC can more easily dissipate any heat buildup, which is known to be responsible for performance degradation. This is particularly important for the use of SiC-based detectors as X-ray beam position monitors (XBPMs) in syncrotron facilities, where interaction with high-intensity beams results in heat loading of the device. Although the thermal conductivity of SiC is about four times lower than that of diamond (22 $Wcm^{-1}K^{-1}$), initial studies of SiC as XBPMs show performance comparable to that of thin commercial diamonds, as discussed in more detail in Par. 4.3.2.

In addition, the high thermal conductivity of SiC allows the temperature to be kept within certain limits during operation, especially when the readout electronics are in direct contact with the detector.

Since the radiation hardness of a solid state detector benefits from the cooling of the device, the good cooling properties of SiC due to its high thermal conductivity can potentially support the radiation hardness of SiC.

2.2 Band gap energy

SiC band gap is 2.36 eV for 3C-SiC, 3.02 for 6H-SiC, and 3.26 eV for 4H-SiC. In general, the higher bandgap of 4H-SiC compared to 6H–SiC and 3C–SiC makes it the first choice for SiC radiation detectors, since most of the processing methods, described in Section 2, are roughly equal between the three polytypes.

The above gap values refer to room temperature, since the band gap decreases with increasing temperature: $Eg - Eg_0 = \frac{\alpha T^2}{\beta + T}$

In this semi-empirical formula reported in [3], Eg_0 is the band gap at 0° K, T is the absolute temperature, and α ($8.2 \cdot 10^{-4} eVK^{-1}$) and β ($1.3 \cdot 10^3 K$) are fitting parameters. The band gap also depends on the doping density, decreasing at high doping levels (above $10^{19} cm^{-3}$).

Thanks to the large energy gap, SiC detectors are characterized by low leakage currents, even at high reverse

TABLE 1 4H-SiC properties at room temperature compared to Si, diamond and GaN.

	Si	4H-SiC	Diamond	GaN
Atomic number[*Z*]	14	14/6	6	31/7
Density [g/cm^3]	2.33	3.22	3.51	6.15
Relative permittivity – ϵ_r	11.9	9.7	5.7	9.6
Energy gap [*eV*]	1.12	3.23	5.5	3.39
e – h pair creation energy [*eV*]	3.6	7.6–8.4	13	8.9
Displacement Energy [*eV*]	13–15	30–40	43	20
Breakdown electric field [*V/cm*]	$3 \cdot 10^5$	$3–4 \cdot 10^6$	10^7	$4 \cdot 10^6$
Electrons mobility μ_e [cm^2/Vs]	1450	800	1800	1000
Holes mobility μ_h [cm^2/Vs]	450	115	1200	30
Saturated electron drift velocity [*cm/s*]	$0.8 \cdot 10^7$	$2 \cdot 10^7$	$2.2 \cdot 10^7$	$1.4 \cdot 10^7$
Thermal conductivity [*W/Kcm*]	1.5	4.9	24–25	2.5

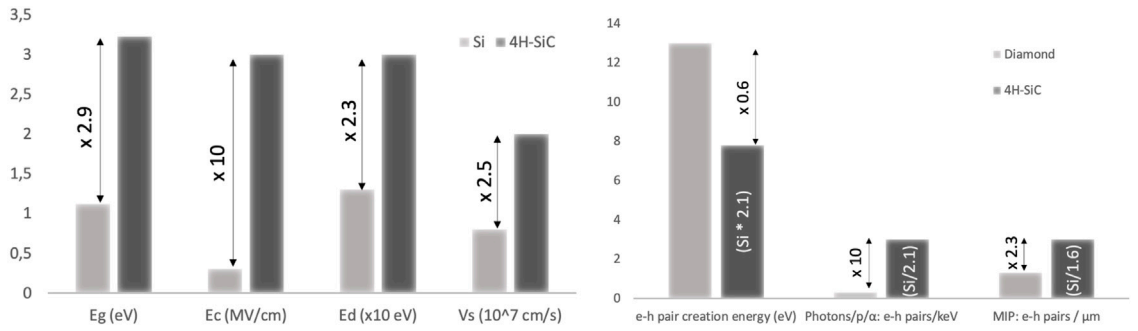

FIGURE 1
Some SiC properties relevant for its use as detection material compared to Si (left) and diamond (right). High Schottky/pn barriers, low thermally generated currents, and visible-light blindness are all results of a wide bandgap (E_g). The high critical field (E_c) implies: high bias voltage and no guard rings. High electron saturation velocity (v_s) means fast signals, short charge transit time, and low charge trapping probability. An high atom displacement energy (E_d) is synonymous of a potential radiation hardness. Finally, a large number of electon-hole (e-h) pairs produced per unit of energy/path is a prerequisite for high detector signals.

bias, and are therefore very low noise. At room temperature, typical commercial 4H SiC Schottky diodes have leakage current densities as low as 347 pA/cm^2 at 403 kV/cm [10]. The lowest leakage current density for a SiC detector reported in the literature to date is 1 pA/cm^2 at 103 kV/cm [11].

Because of the wide bandgap, the intrinsic carrier density at room temperature is extremely low (0.13 cm^{-3} in 3C-SiC, $5 \cdot 10^{-9} cm^{-3}$ in 4H-SiC, $10^{-6} cm^{-3}$ in 6H-SiC), allowing the use of SiC devices at high temperatures with low leakage current.

Finally, the wide band gap makes SiC sensors insensitive to light. This aspect is particularly important for at least two applications of SiC detectors: in the detection of UV radiation under conditions where the signal can be completely obscured by ambient light in the visible spectrum (paragraph 4.3.1), and when the desired signal from ionizing particles can be overwhelmed by low-energy X-rays produced in plasma-generated beams (paragraph 4.5).

2.3 Optical absorption

SiC is an indirect bandgap semiconductor, i.e. maximum-energy states of the valence-band state and minimum-energy states of the conductive-band have different momentum. As a result, a photon with exactly the same energy of the band-gap cannot generate a direct transition between the two states. The change of electron momentum can happen only by interactions with the lattice vibrations or phonons. The extra requirement of a phonon makes the probability of photon absorption with energies close to the band gap relatively low. The higher is the energy of the incident photon with respect to the bandgap, the higher will be the probability of finding pairs of valence and conduction band states with the same momentum and separated by an energy equal to the photon energy. For this reason, the absorption coefficient of a SiC detector increases as the energy of

the incident photons increases, and the photon penetration depth decreases as the wavelengths decrease (Par. 4.3).

The lowest photon energy at which a transition between conduction and valence band states can occur determines the so-called absorption edge of SiC. Some numbers that can be used as reference when characterizing SiC by optical techniques or when SiC are used as photodetectors are [3]: the penetration depth, defined as $1/\alpha_{opt}$, where α_{opt} is the absorption coefficient, is 145 μm at 365 nm (3.397 eV, Hg lamp), 7.4 μm at 325 nm (3.493 eV, 3HG Nd-YAG laser), and 0.7 μm at 244 nm (5.082 eV, 2HG Ar ion laser) for 4H-SiC at room temperature. It is worth noting that SiC has about ten times the absorption of diamonds for X-rays of 8 keV, i.e., 650 versus 70 μm attenuation length. Although diamonds are more transparent in this energy range, the transparency of SiC is still high enough to allow their use as X-ray beam position monitors (XBPMs) with an acceptable low interference with the beam, as discussed in Par. 4.3.2.

2.4 Carrier mobility, lifetime, drift velocity and ionization rates

The low-field electron and hole mobility decreases with increasing temperature and/or increasing donor and acceptor density. Comparing the 4H and 6H politypes at a given dopant density, the hole mobility is only slightly higher in the first politype, while the electron mobility is almost twice as high. This property suggests that the 4H-SiC politype is a better choice for radiation detection, since higher carrier mobility allows more efficient charge collection and thus larger signals. In 4H-SiC, the electron mobility along the c-axis is ~1200 $cm^2\ V^{-1}\ s^{-1}$ at room temperature and about 20% higher along the perpendicular axis. 6H-SiC exhibits a stronger anisotropy.

Another important property of the material for detection performance is the lifetime of the carrier. The latter depends strongly on the type and concentration of defects in the epitaxial layer, especially at low doping concentrations [12]. Carrier lifetime tends to increase with increasing doping concentration (N), as also observed for Si and Ge with a phenomenological $1/N$ dependence as in Ge [13]. Indeed, the probability of thermal e-h recombination due to defect levels in the band gap is higher in heavily doped devices.

The so-called defect engineering represents a promising way to limit the concentration of recombination defects and thus increase the carrier lifetime. In this respect, important results have been published in Refs. [14, 15], where an improvement of lifetime by a factor of two was achieved by high-temperature oxidation (~ 1200°C) followed by removal of the oxide layer on the SiC top layer (~ 50 μm thick).

The drift velocity of charge carriers passes through different regimes depending on the strength of the applied electric field (E): at low electric fields, it is proportional to E; as E is increased, the drift velocity begins to increase nonlinearly and eventually becomes saturated. The saturated drift velocity decreases with increasing temperature. At room temperature, the saturated drift velocity is $2.2 \cdot 10^7$ cm/s and $1.9 \cdot 10^7$ cm/s for n-type 4H-SiC and 6H-SiC [3], respectively. The high saturation velocity of the charge carriers (200 $\mu m/ns$ versus 100 $\mu m/ns$ for Si) leads to fast signals and, in general, potentially more efficient charge collection when defects are present in the lattice (Section 5).

The ionization rate is the number of impact ionization events initiated by an electron (or hole) per unit length traveled. It is a strong function of the applied electric field E. Ionization rates for electrons and holes in 4H-SiC have been measured in Ref. [16] and can be expressed as [3]:

$$\alpha_e(E) \simeq 1.69 \times 10^6 \left(cm^{-1}\right) exp\left(\frac{-9.69 \times 10^6 \left(V cm^{-1}\right)}{E}\right)^{1.6} \quad (1)$$

$$\alpha_h(E) \simeq 3.32 \times 10^6 \left(cm^{-1}\right) exp\left(\frac{-1.07 \times 10^7 \left(V cm^{-1}\right)}{E}\right)^{1.1} \quad (2)$$

Two interesting aspects are worth to be underlined. Firstly, ionization rates in SiC are orders of magnitude below those in Si at a given field [3]. Secondly, holes have an higher ionization coefficient than electrons, which has an impact on the design of SiC-based APD, as discussed in Paragraph 4.3.1. In Silicon, it is the opposite: $\alpha_e(E) > \alpha_h(E)$. As discussed in Ref. [16], the strong suppression of impact ionization by electrons in 4H-SiC may seem quite strange. One should expect electrons to "heat" more efficiently than holes in high electric fields due to their lower effective mass and higher mobility. The authors suggest as a possible explanation the energy bandgap structure of 4H-SiC: the valence band of 4H-SiC is somewhat more complicated than that of cubic materials, with the upper valence subbands wide and continuous. This makes the impact ionization by valence-band holes much more efficient than by conduction band electrons in 4H-SiC (and 6H-SiC as well) [16].

2.5 Breakdown electric field strength

When the reverse bias in a pn junction or Schottky barrier is increased, the leakage current increases due to the generation of e-h pairs and the junction eventually breaks down. The critical electric field strength (cefs, or breakdown electric field strength) depends on the doping concentration. The higher this is, the more the cesf decreases. There are two reasons behind this behaviour: when the doping concentration increases, the width of the depleted region becomes small (Section 4) and thus the distance over which charge carriers can be accelerated becomes short; at the same time, a higher doping density means a higher concentration of impurity centers and thus a lower mobility of charge carriers (Par. 2.4). The cefs of 4H- and 6H-SiC range roughly from $2 \cdot 10^6$ V/cm to $5 \cdot 10^6$ V/cm for doping densities from about $10^{18} cm^{-3}$ to about $10^{15} cm^{-3}$. These

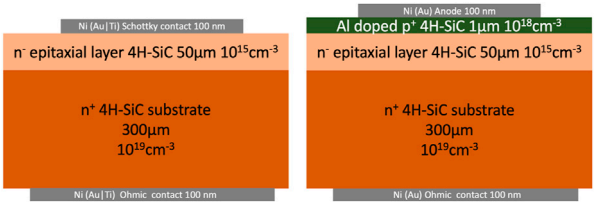

FIGURE 2
Schematic layout of two SiC detectors. The represented materials, thicknesses, doping type and densities are typical for this kind of device, though they can vary depending on the specific case. Left: Scheme of a SiC Schottky diode. The represented detector has four layers (from bottom to top): a Ni thin layer (usually prepared by thermal vacuum evaporation) forming the ohmic back electrode; a n^+ heavily doped conducting substrate wafer; a n^- layer of high-quality lightly doped epitaxial material, usually grown by CVD technology (Par. 3.1.2); and a Ni thin layer forming the Schottky electrode. Right: Scheme of a standard n-type 4H-SiC p-n diode where an heavily doped p^+ layer forms the junction with the n^- epitaxial layer.

values are about eight times higher than Si for a given doping density (three/four times higher for 3C-SiC due to its smaller band gap), making SiC very attractive for power device applications. In addition, SiC's cefs allows it to operate at high reverse bias voltage. This property enables the application of high electric fields, which reduce the transit time of charge carriers and thus the probability of trapping. For example, over-biasing of detectors after radiation damage can increase the CCE (Paragraph 5.1). To limit the required operating voltage of SiC detectors, the doping level of the epilayers is kept low, about two orders of magnitude lower than that of the substrate, as described in Section 4.

3 SiC detector fabrication

A SiC detector is made of different building blocks. A typical epitaxial layer design of a SiC detector based on a Schottky contact is shown in Figure 2 (Left).

It consists of an epitaxial layer, with thicknesses ranging from a few μm up to 250 μm, doped with Nitrogen (n-) with typical concentrations of the order of $10^{15} cm^{-3}$ or less [17]. Much higher dopant concentration, of the order of $10^{18} cm^{-3}$, is present in the conducting SiC substrate of thicknesses of about 300–350 μm. A metallic ohmic contact, usually made of Gold, Titanium or Nickel (or combinations of them) is applied to the substrate on the back of the detector. The front contact can be directly a Schottky contact using a suitable metal such as nickel, or a metal applied to the p^+ layer in $p-n$ junctions (Figure 2 - Right). The latter is formed by diffusing or implanting materials such as aluminum, phosphorus, or boron [18]. $p-n$ structures are generally more difficult to fabricate and are reported, for example, in Ref. [19].

Detailed reviews on the different ingredients of a SiC detector recipe can be found in Refs. [4,5,9,20–24]. Although a detailed description of the fabrication techniques of a SiC detector is behind the scope of this paper, this Section summarizes the main aspects of the growth/deposition techniques and the properties of the above-mentioned building blocks.

3.1 SiC growth techniques

3.1.1 Bulk growth

Nowadays, the most common growth technique of SiC wafer (bulk growth) is the Physical Vapor Transport (PVT) method [25]. Gaseous species of Si, Si_2C and SiC_2 produced from a polycrystalline SiC powder condense on a crystalline seed at temperatures exceeding 2000°C in argon atmosphere at pressures of 15–50 mbar. The process is basically based on the temperature gradient between the heated SiC powder and the cooler SiC seed and allows to reach growth rates of 200–1000 $\mu m/h$. Other recent techniques based on PVT are the Modified PVT (M-PVT) [26] and the Continuous Feed PVT (CF-PVT) [27].

An alternative method is the High Temperature Chemical Vapor Deposition (HT-CVD) [28] in which precursor gases, such as silane (SiH_4) and ethylene (C_2H_4), are used in a more homogeneous temperature profile (1800–2300°C). This method takes the advantage of the high purity of the precursor gases and their continuous supply which gives direct control over the C/Si ratio and doping incorporation. The Halide CVD (H-CVD) [29] is a recent growth technique that allows to achieve high purity SiC with low impurity levels and semi-insulating wafers with high electrical resistivity.

A technique which is still not at the level of industry but is rapidly grovwing is the Top Seeded Solution Growth (TSSG) [30, 31]. TSSG is a liquid phase growth that allows to produce high quality crystal SiC boules. A graphite crucible is used as carbon source that is dissolved in a Si-based melt and transported by diffusion and convection towards a SiC seed in Argon gas at atmosperic pressure, and growth temperatures of 1750–2100°C. The low solubility of Carbon in the Si melt, even at high temperature, and the absence of stoichiometric SiC liquid phase at atmospheric pressure, represent two complications of this technique.

3.1.2 Epitaxial layer growth

Even the state-of-the-art SiC wafers suffer for the presence of high defects and doping concentrations. Therefore, they can be used only as the substrate to support the epitaxial layer, i.e. the active region of the detector. The most common choice in SiC detectors is to growth an epitaxial layer of the same politype of the substrate (homoepitaxially), though examples of heteroepitaxially exist (i.e. 3C-SiC on Si substrates).

Epitaxial growth of SiC can be performed with several techniques: Chemical Vapour Deposition (CVD), Sublimation

Epitaxy (SE), Liquid Phase Epitaxy (LPE), Vapor-Liquid-Solid (VLS) epitaxy and Molecular Beam Epitaxy (MBE).

The most common SiC epitaxial growth process is CVD [32]. In this technique the growth is carried out inside a heated chamber under a mixture of gases composed of carrier gas (such as hydrogen, argon) and precursors (such as silicon and carbon-containing gases). Once heated, the latter decompose into reactive species that will diffuse onto the substrate where additional chemical reactions are responsible for the epitaxial layer growth. Typical SiC-CVD homoepitaxy processes of 4H/6H-SiC have growth rates ranging from some μm up to ~ 50μm per hour. Typical pressures and temperatures involved are in the range 1–960 mbar and 1500–1650°C, respectively [5].

SE technique [33] is based on the same principles of CVD with a reduced distance between the source and the substrate. In general high growth rates can be achieved (e.g. 200 μm/h) at the cost of a lack of control on thickness and doping uniformities.

LPE technique [24] usually makes use of a temperature gradient between the substrate and the melt, and an additional chemical element to increase solubility of the silicon melt. Some detectors fabricated with this technique have been tested with alfa particels as reported in Par. 4.2.

VLS [34] is s relatively new technique based on gas-liquid and liquid-solid interfaces that works at lower temperatures (< 1400°C) and allows higher aluminum incorporation. The growth is triggered when a supplied hydrocarbon decomposes at the liquid-vapor interface and diffuses through the Si melt to the solid-liquid interface.

In the MBE technique [35] precursors are supplied by sputtering or solid source heating and the growth happens under high vacuum conditions. It allows to growth very thin layers at a reduced growth rate ($< 1\ \mu m/h$).

Some of the main properties of the epitaxial layer that affect the quality of SiC sensors as radiation detectors are the net doping concentration, thickness uniformity as well as type and concentration of defects. These properties depends on CVD growth parameters such as C/Si ratio, pressure and temperature, carrier gas flow and growth rate. In particular, for 4H and 6H-SiC homoepitaxial growth, it is crucial to control the C/Si ratio in the gas phase and polish the substrate at an angle (tilt angle) of 8° (6H) and 3.5° (4H) off the basal plane [5]. Also the optimization of pre-growth treatments and epitaxial growth initiation strongly affect the quality of the epitaxial layer [5].

Advances in the grow techniques have led to a continuous increase of epilayer thickness, improving the capability to detect more penetrating radiation with SiC detectors. The highest reported thickness to date is 250 μm [17]. This n-type 4H-SiC epitaxial layer was grown by hot wall CVD on a 350 μm thick 4H-SiC substrate (100 mm of diameter) with a mean micropipe density (MPD) of 0.11 cm^2. Discussion of the performance of epitaxial layers of such thickness in Schottky diodes used as radiation detectors are reported in Par. 4.2.2.

Moving toward the opposite direction, i.e. towards very thin SiC sensors, a recent technique has been developed to fabricate thin epitaxial membranes on 4H-SiC substrates, opening the possibility of using SiC as X-ray beam position monitors in syncrotron facilities (Par. 4.3.2) and/or as diagnostic detectors for flash radioterapy (Par. 4.6). In general SiC is very resistant against traditional chemical etching methods. The new tecnique consists in a electrochemical etching (ECE) in hydrofluoric (HF)-based solutions. ECE is an oxidation/oxide removal process obtained by dipping SiC samples in HF solution and electrically supplying holes for the oxidation through the back metal contact [36]. This process is able to remove selectively the thick highly doped ($\geq 1 \cdot 10^{18} cm^3$) substrate, saving the low-doped n-type layers. In this way it is possible to produce membranes as uniform and thin as the growth epitaial layer. In particular, an etching selectivity ≥ 1000: 1 can be achieved with respect to low doped $5 \cdot 10^{13} cm^3$ layers. Using this new technique SiC Schotky diodes and p-n junctions have been constructed, with thicknesses $< 1\ \mu m$ [37].

3.1.3 Dopant in SiC epitaxial layers

Besides having an high quality epitaxial layer, another crucial parameter in the construction of SiC detectors is the control of its doping level, which implies the reduction of unintentional doping. The latter is usually n-type, caused by nitrogen atoms [5]. Inclusion of dopants in the SiC matrix is based on their atomic size. Nitrogen or phosphorus are usually used for n-type doping, with nitrogen substituting at the C lattice site and phosphorous at the Si lattice site. Aluminum is commonly used for p-type doping, substituting at the Si lattice site. Therefore by increasing C/Si ratio in the silane and propane gases during CVD growing suppress the Nitrogen incorporation and reduce the net doping concentration [5, 23].

C/Si is not the only parameter since, in general, dopant incorporation depends also on other process parameters, crystal orientation and eventually also the reactor geometry. For example, the nitrogen incorporation is reduced by decreasing the system pressure [5].

Tuning the different parameters involved, large range of doping concentration (10^{14}–$10^{20} cm^{-3}$) can be achieved, though lower concentrations are preferred when SiC are used as radiation detectors so to minimize the value of reverse bias needed to reach a significant depleted thickness, avoiding to increase the junction leakage current too much and so the device noise.

The considerable advances made in the last years in controlling the doping of epitaxial layer led to the following state-of-the-art values: a 4H-SiC epitaxial layer 70 μm thick, with a uniform (within 10%) unintentional doping as low as $4 \cdot 10^{13} cm^{-3}$ [5].

3.1.4 Defects in SiC

Perturbations of crystalline periodicity create potential wells in which charge carriers can be trapped. The probability that a

defect will trap a charge carrier is quantified by the so-called capture cross section [38]. The time an electron or hole spends in a trap before being re-emitted into the conduction or valence band depends on how strong the lattice perturbation is. In this regard, trapping states can be classified as follows: shallow states (weak perturbations) with $O(0.1)eV$ binding energies and deep states (strong perturbations) with $O(1)eV$ binding energies [39]. The presence of trapping defects in SiC in the epitaxial layer can reduce the collection of charges generated by incident radiation in two ways. On the one hand, continuous trapping and de-trapping events delay the flow of drifting charges that cannot be fully collected during the signal integration time; on the other hand, a trap containing a charge carrier can attract a carrier of the opposite charge, leading to recombination with multiphonon emission [38].

Impurities and defects in the crystalline matrix of the SiC wafers do not propagate into homo-epitaxial layers. An exception is represented by screw dislocations, like micropipes, whose presence can result in an early breakdown of the diode [5, 40].

Electrically active deep-level defects arise mainly during growth of the semiconductor material, but can also form during processing by ion implantation and/or irradiation of the detector (Section 5).

Actually, defects in the epitaxial layer are generated by unoptimized growth conditions, non-ideal wafer surface finish, or contamination. They are in the form of dislocations and stacking faults. The latter can be minimized in 4H-SiC epitaxial layers, not only improving the substrate surface preparation, but also increasing the growth temperature to 1600°C and lowering the growth rate to about 15 $\mu m/h$ [5, 41, 42].

Defects in SiC and especially in 4H-SiC have been extensively studied by many techniques such as electron paramagnetic resonance (EPR), photoluminescence (PL), deep-level transient spectroscopy (DLTS), and Laplace DLTS (L-DLTS) [39, 43, 44].

Donor and acceptor states associated with carbon vacancy (V_c) are referred to as $Z_{1/2}$ and $EH_{6/7}$, respectively. They dominate over other types of defects in the as-grown 4H-SiC material [9, 17, 45, 46]. The V_c defect has a rather low formation energy of 4.8 eV [47] and forms during high temperature annealing (without irradiation). Typical concentrations of $Z_{1/2}$ in the as-prepared material are 10^{11}–$10^{13} cm^{-3}$. The defect appears as a peak with a maximum at about 320° K in the DLTS spectrum [9]. A broad peak in the DLTS spectrum at about 650° K is the signature of the $EH_{6/7}$ deep level defect[9].

Kleppinger et al [17], studied defects present in very thick epitaxial layers (250 μm) grown CVD. The two peaks observed by the authors in the 80 to 790°K range at 0.62 eV and 1.43 eV correspond to the $Z_{1/2}$ and $EH_{6/7}$ defects, respectively. They had low concentrations on the order of $10^{11} cm^{-3}$ and small capture cross sections of $10^{-15} cm^2$. In particular the small capture cross sections indicate that the observed defects are, on average, related to single atom rather than clusters. This is particularly important for SiC devices where the effect of defect levels on the detector performance depends on the so-called trap's attenuation constant, a combination of trap concentration and capture cross section.

Some promising techniques have been explored to control the concentration of V_C defects. The authors of Refs. [14, 15] suggested that self-interstitials injected into SiC during oxidation are able to annihilate V_C defects and reduce their concentration to a level below $10^{11} cm^{-3}$. Annealing of SiC encapsulated in a carbon-rich pyrolyzed resist film [47, 48], or ion implantation [49–51], are promising techniques worth to be mentioned.

3.1.5 Material characterization

There are many techniques employed to characterize and asses the quality of SiC materials. A review can be found in Ref. [5].

Photoluminescence spectroscopy (PL) is used to determine impurities and defect types in thick epitaxial layers, even when they are present with very low concentrations. The material is illuminated by photons with energy higher than the bandgap at helium temperature (4.2°K) or below and the luminescence spectral response is measured.

The X-ray-beam-induced current microscopy (XBIC) uses x-rays of a few keV energy from a synchrotron source. In this technique the x-ray induced photocurrent is measured as a function of the beam spot on the sensor surface with micrometer resolution.

Thanks to the use of the more penetrating light ion beams (H or He), the Ion-beam induced charge (IBIC) microscopy technique allows the investigation of deep active defects. Low current (less than 1 fA) and highly focused (down to 1 μm) beams are used. The latter induce a current or a charge in the sensor that is measured as a function of beam position on the sensor, allowing the production of charge collection efficiency maps.

Finally, the characterization of deep level defects is based on the measurement of the time constants of the thermal emission transient of current charge carriers. The techniques used are: thermally stimulated current spectroscopy (TSC), deep-level transient spectroscopy (DLTS - transients of capacitance to detect majority carrier traps), photocurrent induced transient spectroscopy (PICTS - transients of photocurrent to detect majority and minority carrier traps), and photo-DLTS (P-DLTS).

3.2 SiC contacts and passivation

3.2.1 Ohmic contacts on SiC

Ohmic contacts are used to carry electrical current, ideally with no parasitic resistance. Several metals deposited on a clean SiC substrate with high doping concentration form ohmic contacts in the as-deposited state [22]. Moreover, it is easier to obtain low resistance contacs on heavily-doped wafers. Thus, to reduce the ohmic contact resistance, an increase in doping

concentration in the region near the semiconductor surface where metal contact is needed. Contacts with lower resistance are usually obtained on n-type 4H-SiC ~ $10^{-5}\Omega cm^2$ than on p-type 4H-SiC ~ $10^{-4}\Omega cm^2$ [5]. For contacts of p-type 4H-SiC, a higher dopant concentration than n-type is required since practical metals form larger potential barriers for holes than for electrons and the energy levels of acceptors such as Al (0.23 eV from the valence band maximum) is much larger than those of donors such as N (0.06 eV from the conduction band minimum) [52].

Changing the Ohmic contact metal, changing the annealing process, and using special surface treatment technologies are all ways to further reduce Ohmic contact resistance [53]. Annealing, in particular, causes a metal-carbide/silice reaction to form, which causes the metal-semiconductor interface to expand and roughen, increasing conductivity through the contact. For a typical 4H–SiC detector ohmic contact obtained by depositing Ti/Pt multilayers of thickness in the range of 500–1500 A, a fast (30 s) heat treatment at 950°C in argon atmosphere is an example [5].

Nickel is also an excellent ohmic-contact metal on 4H-SiC. Depositing 50–100 nm-thick layers, annealing at ~ 1000°C, for order of 1–3 min, different research groups obtained specific contact resistance between 3 and $9 \cdot 10^{-5}\ \Omega\ cm^2$ [53]. The authors of Ref. [53] compared rapid thermal annealing (RTA) and pulsed laser annealing (PLA). They observed that Ni/SiC interface of the PLA sample contained more Ni_2Si, indicating that more carbon clusters and carbon vacancies were produced. Carbon clusters help to increase the conductivity, and carbon vacancies help to increase the tunneling probability. Works on PLA reported in Ref. [53] indicate resistances between $1.97 \cdot 10^3\Omega cm^2$ and $5 \cdot 10^5\Omega cm^2$ using laser densities of $4.7\ J/cm^2$ and $6\ J/cm^2$.

Formation of low resistance contacts to p-type 4H-SiC using laser doping with an Al thin-film dopant source is reported in Ref. [52]. Al doping to the concentration as high as $5 \cdot 10^{21} cm^{-3}$ have been obtained at room temperature. The contact made of Ti/Al metallization provides an ohmic contact whose specific contact resistance is as low as $4 \cdot 10^6\Omega cm^2$ without additional heat treatment.

3.2.2 Schottky contacts on SiC

Almost all the contacts between unannealed metal and a lightly doped SiC are rectifiyng, due to the wide bandgap of this latter. Metals used is SiC detectors are usually Ni or Au [5]. When using SiC Schottky diodes as radiation detectors, there are two important factors related to the junction: the quality of the metal-semiconductor interface and the area of the contact [5]. In the first case, disuniformities and defects reduces locally the junction barrier, exponentially increasing the current. The bad consequences are an increase of the leakage current, that ideally should only be due to thermo-generated carriers over the junction barrier, and a reduction of the breakdown voltage.

Current-voltage (IV) and capacitance-voltage (CV) measurements allow to extract the value of the barrier height together with the diode ideality factor. The SiC Schottky junction barrier height depends weakly on the metal-semiconductor workfunction difference [5]. More crucial is the role played by the surface state and process recipy which include heat treatment processes [54, 55]. Process details are for example described in Ref. [56] where low reverse currents are obtained in low doped ($\approx 6 \cdot 10^{13} cm^3$) Schottky diodes at biases much higher than the full-depletion bias (100 V).

Concerning the Schottky contact area, usually determined by the opening of the mask used for metal deposition, common values in SiC detectors are between 1 and 20 mm^2[9].

Finally, the use of thin contacts is important for high-resolution spectroscopy measurements. Energy loss and straggling due to the Schottky contact need to be evaluated for energy resolution measurements, especially for $Z \geq 2$ ionizing particles, as discussed in Paragraph 4.2.3.

3.2.3 SiC passivation

The majority of the passivation materials utilized in SiC devices are derived from silicon (Si) technology. SiC has the distinct benefit of being the only compound semiconductor that can be thermally oxidized to yield high-quality SiO_2. The following equation describes the thermal oxidation of SiC:

$$SiC + 3/2O_2 \rightarrow SiO_2 + CO. \quad (3)$$

Using the Si density in SiC as a guide, the amount wasted during thermal oxidation of SiC may be determined to be 46%, which is similar to the value for thermal oxidation of Si. To grow 100 nm of SiO_2 on SiC, for example, 46 nm of SiC must be consumed [3].

Most carbon atoms in SiC are lost during thermal oxidation and diffuse out as carbon monoxide (CO) molecules, while a tiny percentage diffuses into the SiC bulk area, reducing carbon-vacancy-related defects [44]. However, carbon atoms are thought to persist around the oxide/SiC contact in the thermal oxide, which is not fully devoid of carbon. In SiC, the oxidation rate depends on temperature, if it is a wet or dry process, and is greatly influenced by the crystal face [3].

Al-based passivations have been studied and compared to the conventional SiO_2 [57]. A variety of dielectrics were coated on unterminated 4H–SiC Schottky barrier diodes, including sputter deposited aluminum nitride (AlN_x), hydrogenated aluminum nitride (AlN_y:H), and aluminum oxide (AlO_z) with a wide range of dielectric constants. Because a bigger dielectric constant has a direct influence on lessening the electric field enhancement at the Schottky contact corner or peripheral, the effects of increasing dielectric constant on leakage currents were investigated. Results show that diodes with a passivation layer consisting of both a thermal oxide interfacial layer SiO_2 and a deposited layer of AlNy:H have a remarkable reduction in leakage currents of more than two orders of magnitude and an increase in Schottky barrier height of as much as 0.2 eV. This is due to a reduction in surface states of more than 30% as a result of the AlNy:H passivation.

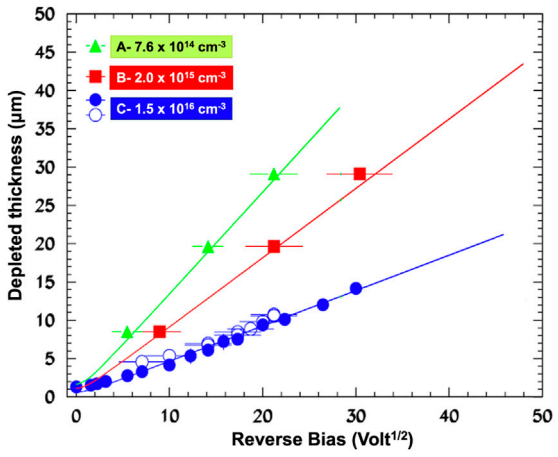

FIGURE 3
Thickness of the depleted epitaxial layer as a function of the applied voltage. Data from Ref. [58] are obtained using SiC Schottky diodes with three different epitaxial doping concentrations (reported in the figure). The effect of the doping concentrations is evident: the lower is the concentration the lower is the bias needed to deplete the same thickness of the diode. Lines represent calculations from Eq. 4 obtained using a SiC static permittivity $\epsilon_r = 9.66\epsilon_0$ and a Schottky barrier height $V_{built-in} = 1.5V$.

Al based passivations outperform traditional SiO_2 passivations, reducing leakage current by at least twice as much due to reduced edge associated tunneling leakage currents. Other benefits of Al-based passivations include improved heat dissipation and the suppression of surface traps due to high thermal conductivity. However, diodes with just the deposited Al based passivation and no interfacial thermal oxide layer, on the other hand, displayed poorer performance, which was ascribed to the poor interface, higher leakage through the dielectric as a result of lower band offset, and sputter-induced surface damage.

4 SiC radiation detectors

The 4H politype produces the majority of SiC-based radiation detectors, with Schottky contacts being the most common. When a reverse bias is applied (negative bias) between the Schottky (or p contact) and the ohmic contact, the region of the epitaxial layer depleted from charge carriers forms the active layer of the detector. The thickness (d) of the latter is determined by the applied bias (V) and doping concentration (N) as follows:

$$d \cong \sqrt{\frac{2\epsilon\,(V_{built-in} + V)}{eN}} \tag{4}$$

where e is the electron charge, $V_{built-in}$ the junction barrier height, and ϵ the SiC dielectric constant. It is clear from this relationship that there are two ways to thicken the active layer. One is to increase the reverse bias, though this solution might be constrained by an upper limit (~ 1000 V) in order to protect the electronic chain and the bonding wires from discharges. The other option is to reduce doping levels. Nowadays, the minimum doping concentration achievable by state-of-the-art SiC epitaxy is about $10^{13} Nitrogen/cm^3$ [8].

Figure 3 shows the thickness of the depleted region as a function of square root of the reverse bias for three 4H-SiC Schottky detectors with different epitaxial layer doping concentrations. The bias needed to deplete the same thickness is lower for lower doping concentrations, as expected from Eq. 4. It is worth noticing that the biases needed are quite high, i.e. 400 V to deplete only 30 μm of the lightest doped sensors.

4.1 Detection of electrons

Different works have investigated the response of SiC detectors to electrons, i.e. when used as MIP (Minimum Ionizing Particle) detectors. For MIP, the various measurements point to a quantity of produced electro-hole pairs (e-h) on the order of $50(e-h)/\mu m$.

In Refs. [59, 60] the authors investigated the signals of 2.2 MeV electrons generated into 4H-SiC p-n junctions and Schottky barrier, respectively, using a $^{90}Sr\ \beta$ source. Detectors based on n-type, $6 \cdot 10^{13} cm^3$ doped, and 40 μm (nominal) thick epitaxial layers were used in the latter case. In Ref. [5], the charge collected as a function of the applied bias is reported in electron charge units. A bias of ~60 V saturates the collected charge. The latter is about $2090e$ corresponding to $55 \pm 3(e-h)/\mu m$.

A consistent value (51 e/h) is found in Ref. [61], which used semi-insulating 300 μm thick 4H–SiC detectors with ohmic contacts to test them with a $^{90}Sr\ \beta$ source. For a reverse voltage of 500 V, a response of approximately $2000e$ has been measured. Nonetheless, the high density of deep level defects generates a large number of trapping processes, causing the signal to decay rapidly to $800e$ with a decay constant of 14 min.

Bruzzi et al. [62] used a 0.1 mCi ^{90}Sr source to test the charge response of 4H-SiC Schottky barriers. Epitaxial layers with an effective doping concentration and maximum active thickness of $6.1 \cdot 10^{14} cm^3$ and 20.8 μm, respectively, were used, as determined by C-V analysis. In the range of 0–250 V, the pulse height spectrum is measured as a function of the reverse voltage. A bias of ~240 V saturates the collected charge at around $1100e$, which corresponds to $51(e-h)/\mu m$, which is consistent with the results of the previous measurements. Minority carriers also contribute to the signal, as explained in detail in the following paragraph. The minority carrier diffusion length measured at zero bias is $L_p \sim 4\ \mu m$.

4.2 Proton, alfa and heavy ion detection

During the last two decades, SiC Schottky barrier detectors have been extensively studied as ionizing radiation detectors with

TABLE 2 The main detector properties, the type of radiation used, and the detector characteristics studied in the works cited in Par. 4.2.

Ref	Studies	Radiation	Doping [cm^{-3}]	Thickness	Area
[63]	Linearity, ϵ_{SiC}	p 1–2 MeV	1.5, 4.5 · 10^{14}	40 μm	1.8 mm^2 19.6 mm^2 circular
[64]	Linearity CCE Energy res. Timing	α,^{12}C,^{16}O 5–18 MeV	1.5 · 10^{16}	21 μm	2 × 2 mm^2
[13]			7.6 · 10^{14}	37.9 μm	
[58]			2 · 10^{15}	43.7 μm	
[65]	Linearity	α	4.5 · 10^{14}	25 μm	1 × 1 mm^2
	Energy res	3.27–8.79 MeV			2 × 2 mm^2
					3 × 3 mm^2
[66]	CCE	α	1 · 10^{14}	105 μm	0.64 mm^2
	Energy res	5.1–5.8 MeV			circular
[5]	CCE	p	n/a	35 μm	n/a
		1.5.2 MeV			
[17]	CCE	α	0.95–1.85 · 10^{14}	250 μm	8 × 8 mm^2
	Energy res	5.486 MeV			
[67]	CCE	α	1.34 · 10^{14}	20 μm	8 × 8 mm^2
	Energy res	5.486 MeV			
[68]	Energy res	α	1 · 10^{14}	100 μm	15.9 mm^2
		3.18–8.38 MeV			28.3 mm^2
					circular
[69]	Energy res	α	6–10 · 10^{14}	26.55 μm	1 × 1 mm^2
		4.8–7.7 MeV			
[70]	Energy res	α	2.4 · 10^{14}	20 μm	11 mm^2
		5.486 MeV			circular
[71]	Energy res	α	7–8 · 10^{13}	25,50,70 μm	3.14 mm^2
		5.4, 5.9 MeV			7 mm^2
					circular
[72]	Timing	α	6.5 · 10^{13}	115 μm	0.4 × 0.4
		5.486 MeV			mm^2
					pixel

Doping and thickness refer to the epitaxial layer. All the detectors are 4H-SiC Schottky, except for Ref. (Chaudhuri et al., 2021) where MOS (metal-oxide-semiconductor) were used.

protons, alphas, and heavy ions. This paragraph summarizes some of the most important works and outcomes. Despite the fact that the performance of such devices depend on their design, the following general conclusions can be drawn from the various works:

- High degree of linearity between the incident energy of the radiation and the collected signal.
- SiC Schottky diodes can provide 100% Charge Collection Efficiency (CCE)
- When the particle range in the detector is longer than the depleted layer, a contribution from minority carriers is observed in the signal
- Excellent timing properties have been proved with time resolutions as high as 117 ps.
- Spectroscopic performances comparable to standard Si detectors have been observed with energy resolutions below 0.5% and up to 0.25% (FWHM) for ~5.5 MeV alpha particles.

Table 2 summarizes the detector characteristics studied, the type of radiation used, and the main detector properties for each cited work.

4.2.1 Linearity

In Ref. [63] the response of the detectors is found to be linear as a function of the proton energy. The authors also extracted the average energy ϵ needed to generate e-h pairs The value of ϵ is related to the energy of the incident particle (E) and the average number of pair (N_{eh}) created in the active volume of the detector *via* $\epsilon = \frac{E}{N_{eh}}$. E is evaluated considering the energy lost in the detector entrance window and N_{eh} is inferred by measuring the total collected charge Q = q ·N_{eh}. Using a standard Si detector as reference and assuming ϵ_{Si} = 3.64 for protons, ϵ_{SiC} for protons is found to be 7.78 eV.

M. De Napoli et al. investigated the detection of alpha particles and low-energy ^{12}C and ^{16}O ions using SiC Schottky

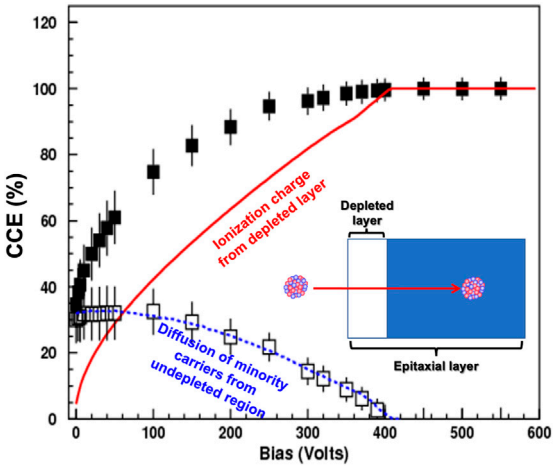

FIGURE 4
CCE of a SiC Shottky diode used to detect 27.7 MeV ^{12}C as a function of the operating bias. The theoretical values obtained from Eq. 5 are represented by a solid line. The contribution of minority carriers diffusing from the undepleted region of the expitaxial layer is represented by the differences between experimental points and theoretical predictions of Eq. 5 (empty squares). This contribution is well fitted using Eq. 6 with an L_p = 5 μm [13].

diodes [64]. A linear best fit of the pulse height vs. particle energy (for alphas, ^{12}C and ^{16}O) yielded a linear correlation coefficient R_2 of 0.998, indicating a strong proportionality between the collected charge and the energy loss in the active layer.

Recently, Bernat et al. [65] also found an high degree of linearity as a function of incident energy (R_2 = 0.99967) up to 6.7 MeV, the maximum energy that allows α to stop within the thickness of the SiC epitaxial layer.

4.2.2 Charge collection efficiency

M. De Napoli et al. studied the Charge Collection Efficiency (CCE) as a function of the applied bias [13]. Starting at 0 V and increasing the bias, the CCE rises as more charges are produced in increasingly thicker depleted regions (Figure 4), as expected. CCE saturates at 100% when the latter reaches a thickness equal to or greater than the ^{12}C range in the detector. The CCE of charge carriers produced in the depleted (drift) region is calculated as follows:

$$CCE_{drift} = \frac{1}{E_0}\int_0^d \frac{dE}{dx}dx \tag{5}$$

where E_0 is the incident energy and d the depleted thickness. The solid line in

Figure 4 represents calculations from Eq. 5. It is evident that they underestimate the measured CCE. The extra-charge, which makes the experimental CCE higher than the calculated CCE_{drift}, result from the collection of minority carriers. The latter are generated by the incoming ^{12}C in the undepleted region, when $d < {}^{12}C - Range$, which diffuses toward the depleted region, where they are collected under the effects of the electric field. The contribution of minority carriers to the CCE is well described by the equation [73]:

$$CCE_{diffusion} = \frac{1}{E_0}\int_d^D \frac{dE}{dx}e^{-\frac{x-d}{L_p}}dx \tag{6}$$

where D is the thickness of whole epitaxial layer and L_p is the minority carrier diffusion length, i.e. the average distance that a minority carrier diffuses before it recombines with charge of opposite sign. $CCE_{diffusion}$ calculations well reproduce the difference between the experimental CCE and the calculated CCE_{drift} (Figure 4). In particular, the L_p values obtained in Ref. [13] are 7 ± 1 μm and 5 ± 1 μm for the heavier and lighter doped SiC, respectively.

A study of the CCE as a function of the reverse bias is also reported by [5]. The CCE saturation observed corresponds to bias voltages (60 and 120 V for 1.5 and 2 MeV protons, respectively) that are equal to or higher than the value required to deplete the active layer up to proton range. Hole diffusion within the drift region contributes to the collected charge in depleted regions shorter than the proton range. A hole diffusion length of L_p = 7 μm and a hole lifetime of 160 ns were obtained from a best fit analysis of the CCE.

A CCE = 100% for bias > 50V is also observed in Ref. [66].

SiC detectors with an exceptionally thick epitaxial layer of 250 μm have been recently tested in Ref. [17] using a ^{241}Am source. The CCEs were measured to be 98–99% and the drift-diffusion model discussed above, used to fit the CCE vs. bias, revealed a L_p = 10 μm.

Finally, it is worth mentioning the recent work of Ref. [67] on Ni/SiO_2/n-4H-SiC vertical MOS (metal-oxide-semiconductor). Despite the presence of the oxide layer, the detectors showed a high CCE of 96% at 40 V (detector depleted to 18 μm, almost equal to the alfa range). The drift-diffusion model discussed above gives a L_p = 24 μm.

4.2.3 Energy resolution

Energy resolution as a function of the applied bias is measured by M. De Napoli et al. in [58] (Figure 5 - left panel). Increasing the bias improves the energy resolution significantly. A plateaou in the resolution is reached for bias values that are equal to or greater than those required to have a depleted active region (d) that is deeper than the ions range (R). The low resolution observed for bias values corresponding to $d < R$ is caused by two factors: incomplete charge collection and the collection of minority carriers from the undepleted region (Par. 4.2.2). The latter generates large fluctuations in the collected charge caused by random recombination of minority carriers before they are collected, as well as the ballistic defect associated with their long collection time. The saturated energy resolution

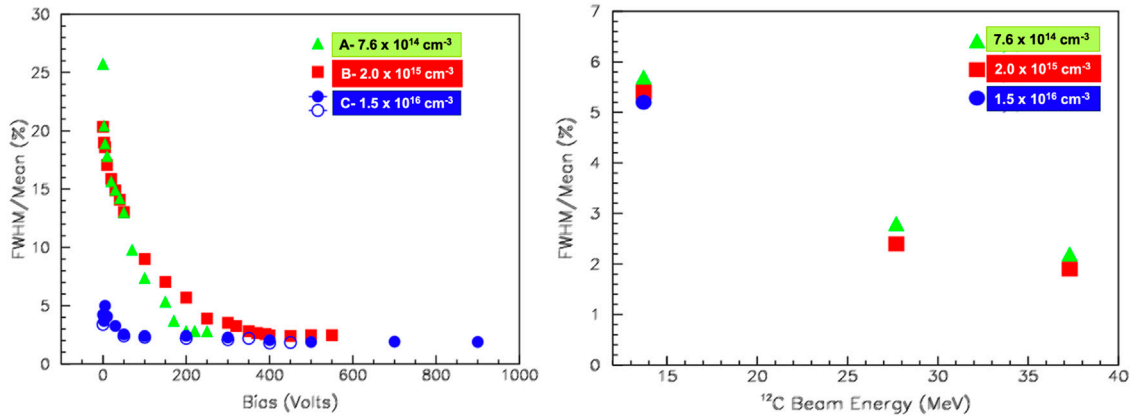

FIGURE 5
Left: Relative energy resolution measured using ^{12}C at 27.7 MeV as a function of the bias for three SiC with different epitaxial doping concentrations. Right: Energy resolution as a function of ^{12}C incident energies, measured in the pulse-height saturation regime. Data are from [58].

for ^{12}C of different energies ranges from 5.5% to 1.7% (Figure 5 - right panel). It varies slightly depending on the doping concentration, and as expected, less doped SiC detectors have better resolutions due to a lower defect concentration.

Recently, Bernat et al. [65] obtained similar energy resolution values: 3% and 3.3% for α of 5.486 MeV (^{241}Am source) and 3.183 MeV (^{148}Gd source), respectively.

The spectroscopic characteristics of 4H–SiC used to detect alpha particles are the focus of other two published works [68, 69].

Authors of Ref. [68] used Schottky diodes with a (9000 A°) gold/(1000 A°)platinum/(800 A°)titanium entrance window. Factors that influence energy resolution have been thoroughly assessed. Measurements from a silicon detector equipped with the same metallic window were used to subtract α straggling due to the entrance window. After the substraction of the electronic and statistical broadening too, the authors inferred an inherent SiC resolution of 0.6% (FWHM of 19.4 keV) for 3.18 MeV alpha particles of ^{148}Gd source.

In Ref. [69] detectors were equipped with a 1000 °A chromium entrance window. The measured resolution for 5.0–5.5 MeV alfas is <20 keV (0.34%) compatible with the value found in Ref. [68], though the straggling caused by the chromium layer was not taken into account.

Another spectroscopic study using alfa particles from a ^{238}Pu source have been recently reported in Ref. [71]. At room temperature, the measured reverse current was <50 pA. For the three detector thicknesses, C-V measurements revealed Schottky barrier heights between 1.09 and 1.3 eV, series resistances between 0.6 and 0.9 $k\Omega$, and ideality factors between 1.33 and 1.55. For alfa at 5.5 MeV, high energy resolution (FWHM) $\simeq$ 0.35–0.4% has been measured for the three epitaxial layer thicknesses.

Kleppinger et al. [17] measured an energy resolution lower than 0.5% at 200 V in their thick detectors.

In Ref. [66] an extremely thin contact of Ni/Au (15 nm) was used to optimize the spectroscopic performance. Leakage currents lower than 0.3 nA/cm^2 at room temperature were observed. The best energy resolution measured is 0.25% (FWHM) for 5.486 MeV alphas at a reverse bias of 200 V.

Chaudhuri et al. [70] obtained another significantly high energy resolution for a relatively large area detector. The detectors are made of a 10 nm thin Ni Schottky contact (circular, with an area of $\sim 11\ mm^2$). At 90 V and room temperature, a leakage current of 3.5 pA was measured. For 5.486 MeV uncollimated α, an energy resolution of 16.2 keV (0.29%) was observed. The recipe behind the good energy resolution achieved consists of the following ingredients: thin Ni window to minimize energy straggling, high Schottky barrier (1.6 eV), diode ideality factor ~ 1, low doping epitaxial layer of high quality (micropipe density $<1\ cm^2$). The white series noise dominates the electronic noise. Since the latter is influenced primarily by the input capacitance, using SiC detectors with a thicker epitaxial layer (i.e. lower capacitance for the same area) would allow for even better energy resolutions.

Still Chaudhuri et al. [67] reported the highest energy resolution ever measured on SiC-based MOS detectors: 0.42% for 5.48 MeV alpha particles. Although good, in general MOS detectors do not yet have the same energy resolution as Schottky barrier detectors. The reason for this is that lifetime killing defects like $Z_{1/2}$ and $EH_{6/7}$ typically have a much higher concentration (at least one order of magnitude).

4.2.4 Time resolution

Among the different studies carried out by De Napoli et al. on SiC detectors, they measured a signal rise-time from the

TABLE 3 Properties of the detectors used in the works cited in Par. 4.3.

Ref	Rad	Det. type	Doping [cm^{-3}]	Thick	Area [mm^2]
[76]	UV	PD, 6H n-p	10^{17}–10^{18}	1–5 μm	1 × 1 2 × 2 3 × 3
[77]	UV	PD, p-n	$1 \cdot 10^{14}$	3.5 μm	1 × 1
[78]	UV	PD, Schottky			5 × 5
[79]	UV	PD, Schottky interdig. struct	$2.7 \cdot 10^{15}$	5.8 μm	1 × 1
[80]	UV	APD	*see* text	*see* text	from 0.05 × 0.05 to 0.21 × 0.21
[81]	UV	APD linear array	*see* text	*see* text	*see* text
[82]	X-ray	Schottky	$1.8 \cdot 10^{15}$	30 μm	3.14, circular
[83]	X-ray	Schottky	$4 \cdot 10^{14}$	20 μm	0.18 × 0.18 0.28 × 0.28 0.38 × 0.38
[84] [85]	X-ray	Schottky	$8 \cdot 10^{14}$	50 μm	8 × 8
[86]	X-ray	Schottky	$16.7 \cdot 10^{14}$	20 μm	0.25 × 0.25
[87]	X-ray	Schottky	$< 10^{14}$	25 μm	0.5 × 0.5
[11]	X-ray	Schottky pixel	$5 \cdot 10^{14}$	70 μm	0.03, circular
[88]	X-ray	Schottky microstrip	$5.2 \cdot 10^{13}$	100 μm	32 strips 2 mm lenght 25/50 μm width
[37]	X-ray	p-n junction ultra-thin	$5 \cdot 10^{13}$	down to 0.5 μm	4 × 4
[89]	X-ray	Schottky	$2.2 \cdot 10^{15}$	30 μm	3.14, circular
[90]	X-ray	Schottky	undoped	115 μm	5, circular

Doping and thickness refer to the epitaxial layer.

preamplifier of 44 ns at 440 V [64]. The measurements were taken with a 45 mV/MeV gain charge preamplifier and ^{12}C ions at 17.68 MeV.

Nanosecond time resolution were measured with 4H-SiC Schottky diodes during the detection of laser-accelerated plasma radiation [74, 75] (Paragraph 4.5). Zhang et al. [72] focused on the timing performance of a 4 × 4 4H-SiC pixel, with pixel of 400 × 400 μm^2 separated each other by a distance of 40 μm. The detector was biased at 300 V, depleting about 70 μm, which was enough to stop alphas from the active volume's ^{241}Am source. Electronic noise is negligible due to the ultra-low dark current (in the range of 2–13 fA at 300 V and room temperature) and the low capacitance of individual pixels (0.5 pF). Timing measurements are performed using a thin (20 μm) plasti scintillator optically coupled to two PMTs. A very good time resolution of 117 ± 11 ps was measured.

Time resolution of SiC is therefore comparable. with that of Si detectors, i.e. O(1/10 nsec) for standard detectors and O(10/100 psec) for detectors optimized for timing measurements.

4.3 SiC sensors for photons

The type and main properties of the detectors used by the cited authors who tested SiC devices as photon sensors are summarized in Table 3. The results of using SiC detectors as UV photodiodes and X-/γ-ray detectors are split into two sub-paragraphs.

4.3.1 UV photodiodes

Pin photodiodes and avalanche photodiodes (APDs) are the most common SiC photodetectors. A pin photodiode can have the following basic structure: the active region is formed by the growth of an n-doped layer on a n^+ substrate, which is in contact with a thin heavily-doped p^+ layer forming the diode junction. The p^+ layer's metal contacts are spaced apart to allow light to pass through, and the surface is coated with an anti-reflective coating. Photogenerated primary carriers are accelerated in APDs, resulting in secondary ionization and signal amplification.

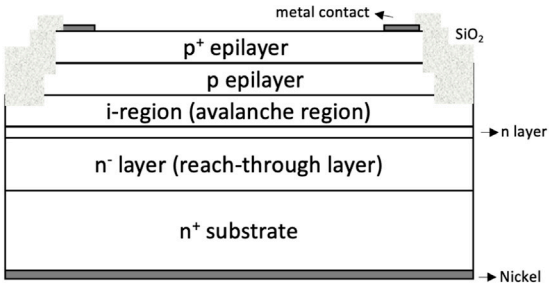

FIGURE 6
Schematic view of a typical APD structure [80]. The reported example is made up of a n^+ substrate, a n^- 2 μm thick reach-through layer (used to increase the quantum efficiency of penetrating UV light), a 0.11 μm n layer, a 0.2 μm intrinsic-region (avalance region), a 0.25 μm p layer, and a 0.2 μm p^+ layer. Doping levels are $4 \cdot 10^{15}$, $1 \cdot 10^{18}$, $1.3 \cdot 10^{18}$, and $3 \cdot 10^{19} cm^{-3}$ for the n^-, n, p, and p^+ layers, respectively.

Usually, the choice falls on the further acceleration of holes instead of electrons due to their higher ionization coefficient (Par. 2.4). For this purpose, an additional thin and heavily doped n layer is included through the n-collection region to generate a region of high electric field where accelerated charges produce secondary ionization. In Figure 6, a sketch of a typical SiC APD structure is shown.

At short wavelengths ($\lessapprox$200 nm) the absorption coefficient of SiC photodiodes is large and few photons reach the charge collection region. At long wavelengths ($\gtrapprox$400 nm) the absorption coefficient is small since photon energies are not enough to produce e-h pairs1 (Par. 2.3) and photons can be also absorbed deeper in the not-depleted volume of the detector. Therefore there is an intermediate wavelength range where responsivity is maximum.

SiC photodiodes can be of the type described above (with n- or p-type epitaxial layers), as well as Schottky diodes with metal silicide thin films [5].

Detectors of the first kind have been investigated by first author et al. [76]. A heavily N-doped epitaxial layer of 0.2 or 0.3 μm thick was used to form the $n^+ - p$ junction. Responsivity is measured between 200 and 400 nm at different temperatures between −50 and 350°C. At room temperature, a responsivity peak of 175 mA/W is observed at about 270 nm with a quantum efficiency of about 70%–85%. This is the so-called "external" quantum efficiency since the responsivity of the device was measured without correcting for reflection and therefore, represents the current generated for a watt of photon flux incident on the device. Very low dark current, even at elevated temperatures, are reported (10 nA/cm^2 for $2 \times 2\ mm^2$ devices at 300°C), indicating that SiC photodiodes can have excellent performance for UV detection even at elevated temperatures.

$p^+ - n$ junction photodiodes obtained by aluminum (Al) ion implantation on low-doped n-type epilayers have been studied as UV detectors by Sciuto et al. [77]. The epilayer was grown on a heavily doped n-type substrate at $1 \cdot 10^{19} cm^{-3}$. Al implantation with a p^+ region 175 nm depth and an activated dopant concentration of about $1 \cdot 10^{19} cm^{-3}$ formed the p-n junction. Dark currents lower than 1 nA/cm^2 have been measured at 90°C. The responsivity observed at 280 nm is 110 mA/W which corresponds to a quantum efficiency of about 50%. Visible blindness $> 10^3$ is also observed. The latter is defined as the ratio between the 280 nm responsivity value and the average responsivity estimated in the visible range 400–600 nm.

A lower quantum efficiency was found by Yan et al. [78] in Pt/4H-SiC Schottky photodiodes. 75 Å semi-transparent Pt was deposited on n^- side to form Schottky contact. A gold contact ring (100 μm) for wire bonding was deposited on the top of the semi-transparent Pt. Leakage current of $5 \times 5\ mm^2$ devices were found to be lower than $10^{-15} A$ at zero bias and room temperature. The quantum efficiency measured is over 30% in the range from 240 to 320 nm. Specific detectivity in the range 210–350 nm was found to be above $10^{15} cm \cdot Hz^{1/2}/W$ with a peak of $3.6 \cdot 10^{15} cm \cdot Hz^{1/2}/W$ at 300 nm.

4H-SiC Schottky photodiodes with a vertical structure have been considered in Ref. [79]. Semitransparent Schottky contacts were obtained by defining self-aligned nickel silicide Ni_2Si micrometric interdigit structures. The definition of 4.8 μm wide Ni_2Si stripes (5.4 μm spaced) was obtained by using selective metal etch and standard optical lithography. The areas directly exposed to the radiation, i.e., the "open area," was 0.37 mm^2. The dark current was about 200 pA at 50 V. In the pinch-off regime they measured a maximum responsivity of 160 mA/W at 265 nm and an UV rejection ratio $> 7 \cdot 10^3$. The latter is defined as the ratio between the values of the responsivity at 256 and 405 nm.

Concerning SiC avalance photodiodes, Yan and others studied the performance of single APD sensors and linear arrays of APD. In Ref. [80] 4H-SiC APD with intrinsic-region widths of 0.105 and 0.285 μm (mutiplication regions) have been investigated using 230–365 nm light using a mercury–xenon (Hg–Xe) lamp. The APD structure is schetched in Figure 6. Responsivities of about 130 mA/W have been obtained at 265 nm, corresponding to quantum efficiencies above 60%. A 40 pixel linear array of SiC APD, each with $4.3 \cdot 10^{-5} cm^2$ of area, is studied in Ref. [81]. The array is 2 mm long, the period of pixels is 50 μm and the pixel spacing 15 μm. Pixels are isolated from each other by 1.5 μm deep mesa. The edge of mesa is passivated by a 40 nm thick high quality thermal oxide and a 1 μm thick LPCVD oxide. A $p^+ - p - n - n - n - n^+$ APD structure is used. The doping concentrations and thicknesses from p^+ to n are: $3 \cdot 10^{19} cm^3$ and 0.2 μm, $1.3 \cdot 10^{18} cm^3$ and 0.25 μm, $5 \cdot 10^{15} cm^3$ and 0.22 μm, $1 \cdot 10^{18} cm^3$ and 0.11 μm, and $4 \cdot 10^{15} cm^3$ and 2 μm, respectively. The substrate is n^+ with a doping concentration close to $10^{19} cm^3$. The optical gain is about $3 \cdot 10^6$, assuming a unity quantum efficiency. The linear arrays show uniform breakdown voltage (120 V for 91% pixels) and low leakage

current. The responsivity in the 250 and 330 nm range is higher than 105 mA/W with a visible rejection ratio >100. The extracted Excess Noise Factor (ENF) varies from about 2–10 for multiplication factor between 5 and 35 with the corresponding k around 0.1–0.2, depending on the device under test. This results show the excellent noise performance of 4H-SiC APDs, indicating that 4H-SiC is an ideal semiconductor for low noise APD fabrication.

4.3.2 X-/γ-ray detection

A large number of studies on the response of SiC detectors to X- and γ-rays have been conducted. Different detector structures have been investigated depending on the type of application, ranging from spectroscopy to beam monitoring and dosimetry: traditional Schottky diodes, microstrips, pixel, and very thin layers. Some general conclusions can be drawn from this diversity:

- In terms of x-γ adsorption, 4H-SiC Schottky barrier detectors with active layers as low as 16 μm thick are sensitive to electromagnetic radiation up to 59.6 keV.
- Energy resolutions as high as ~ 3.6% at 5.9 keV can be achieved
- SiC detectors can measure high-resolution X-ray spectra at high temperatures (up to 100°C) and during temperature changes.
- In terms of transparency, linearity, dynamics, and signal-to-noise ratio, SiC devices have shown comparable or even better performance than commercial polycrystalline diamond as X-ray beam monitors.
- *In vivo* dosimetry is another field where SiC-based sensors have comparable performance to commercial diamonds.

A summary of the results of some selected works that demonstrate the above-mentioned SiC performances is presented in the following.

4.3.2.1 Spectroscopic studies at room temperature

The first experimental results of X-ray spectroscopy by means of SiC Schottky junctions dates back to 2001 [82]. The detector biased at 500 V was used at room temperature to measure the X- and γ-rays energy spectrum from an ^{241}Am source. The main peaks in the spectrum are at 13.9, 17.8, 26.3, and 59.5 keV, with decreasing intensities due to the rapid decrease in detection efficiency as energy increases. The reason for this is the epitaxial layer's thin thickness, which, when combined with the relatively large junction area (3 mm^2), results in a high detector capacitance (16 pF) and thus a significant noise contribution.

In 2007 Lees et al. [83] used a new detector structure, a semi-transparent SiC diode with an "ultra-thin" (18 nm Ni/Ti) Schottky contact, deposited using e-beam evaporation, a gold annular overlayer and a gold corner-contact pad. This new architecture has an ideality factor below 1.05, i.e. totally compatible with those of classic thick structures (1.04–1.06). A result of the high-quality interface between the SiC and the contact. Because of the ultra-thin front contact, which minimizes absorption in the electrode structure, the detection efficiency of low-energy X-rays (<10 keV) is up to 100× higher than in standard Schottky diodes. Furthermore, X-ray spectra from ^{55}Fe, ^{109}Cd and ^{241}Am radioactive sources show promising spectroscopic capability at room temperature (1.47 keV FWHM at 22 keV, ~ 6.7%). Reduced contact thickness comes at the cost of a lower Schottky barrier height (1.05 eV), which means more noise.

An high sensitivity to soft x-rays in the 50 eV to few keV range, and a better energy resolution of 2.1% for 59.6 keV gamma rays were found by Mandal et al. [84, 85]. Detectors were tested with a synchrotron light sourcesat at NSLS (BNL) and using an ^{241}Am source. A very thin ~10 nm Ni Schottky contact was deposited with the sputtering technique. Special bonding technique has been developed to avoid damage on the Ni contact. The sensitivity to higher-energy photons (starting at 2–3 keV) was limited by the active volume thickness (~ 16 μm at 250 V).

As demonstrated by Lioliou et al. in two papers, optimizing the readout electronics, such as the amplifier shaping time and selecting the appropriate preamplifier, is critical for obtaining good energy resolution. They investigated the performance of different SiC diodes as X-ray detectors at 30°C in both current mode and for photon counting X-ray spectroscopy in Ref. [86]. Schottky contacts are made by depositing 3 nm Ti and 12 nm Ni with e-beam evaporation and then annealed at 600°C. A Mo-target X-ray tube was used to test the detectors. The photogenerated current as a function of the applied bias was calculated by subtracting the leakage current (2 nA/cm^2 for 200 V biasing) from the total current. At reverse biases of up to 100 V, measured photocurrents range from 4 to 8 pA. With diodes biased at 60 V, the K_α and K_β peaks in the x-ray spectra of the Mo-target were measured. The measured energy resolution (FWHM at 17.4 keV, Mo K_α) is ~ 8.5%, ranging from 1.36 to 1.68 keV depending on the diode. Stray capacitances near the input of the custom charge preamplifier used are to blame for the low resolution.

4.3.2.2 Spectroscopic studies at high temperature

The capability of 4H-SiC Schottky photodiodes for high-temperature photon counting X-ray spectroscopy [87] was recently investigated by the same group. In particular, ^{55}Fe X-ray spectra measurements were performed from 0°C to 100°C. The devices exhibited low leakage current densities (<200 pA cm^{-2} at an applied electric field of 200 kV/cm and room temperature), a zero band barrier height of 1.358 eV, and an ideality factor that deviated from unity (≃ 2.7). At 50 V applied bias, devices were fully depleted (~ 27 μm). At room temperature, the best energy resolution (FWHM at 5.9 keV) was

1.29 keV, or ~ 22%. When the custom charge-sensitive preamplifier is used at the same temperature as the detector, the energy resolution improves slightly at 0°C (FWHM of 1.20 keV) and decreases at 100°C (2.20 keV, i.e. ~ 37%). Because dielectric noise was the most common source of noise, the preamplifier, rather than the detector, was responsible for limiting energy resolution.

Bertuccio et al. [11] used a custom ultra low noise CMOS preamplifier coupled to a 4H-SiC pixel detector in the T = 30–100°C range to detect X-rays from a ^{55}Fe (5.9 and 6.5 keV peaks) and a ^{241}Am (0–28 keV range) source. A bias of 300 V was used (corresponding to depletion thickness ~ 25 μm and capacitance ~ 1pF). At T = 30°C (~ 3.3%), the measured 5.9 keV line has a width of 196 eV FWHM. Only a slight worsening of the energy resolution is observed at the higher temperature of T = 100°C (for both detector and preamplifier): the measured FWHM is 233 eV (~ 3.9%). F = 0.10 has been calculated as the Fano factor. Finally, during the acquisition of the energy spectrum, the detector was tested under unsteady temperature conditions ranging from 30 to 75°C. With a slight line shift of 0.3 eV and broadening of 6.1 eV at 5.9 keV, the energy spectrum maintained its quality under such variable conditions.

Puglisi et al. demonstrated the use of microstrip SiC detectors as high resolution X-ray detectors in the range 0–60 keV and over a wide range of operating temperatures in a recent paper [88]. The authors characterized 4H-SiC microstrip detectors with a very low leakage current, from about 2 fA at 25°C to 620 fA at 107°C, among the best values measured on SiC detectors. The X-ray spectra in the range 0–60 keV acquired from a ^{241}Am source showed high stability and spectroscopic resolution, with voltages between 80 V and 200 V and temperatures between 20°C and 80°C. Several X-ray lines from Mn, Cu, Np, and Ag, in particular, can be distinguished with enough energy resolution to distinguish K and L lines from neighboring elements. Between the X-ray peak energies and the detector signals, there is a high degree of linearity. Peak positions do not change significantly as the detector bias is increased from 10 to 200 V, the energy resolution improves due to lower capacitance, and the photon rate increases with the square root of the bias due to the wider active region, as expected. At room temperature, the energy resolution measured for the conventional Mn K_α peak at 5.9 keV is 213 eV (~ 3.6%). Given that Si(Li) and silicon drift detectors can achieve 130–150 eV FWHM for the same Mn K_α peak, and Ge detectors can even achieve 115 eV FWHM with liquid-nitrogen cooling, this is an excellent result. Furthermore, only a minor broadening of the lines is observed at 80°C.

4.3.2.3 Beam monitoring

For beam monitoring, the ability to extract information on the X-ray position can be used. SiC has recently been proposed as a promising candidate to replace diamonds in synchrotrons as X-ray beam position monitors (XBPMs). To minimize interference with the beam, XBPMs must be as thin as possible. They must also be able to withstand a lot of heat and absorb a lot of radiation. SiC's high-temperature stability and radiation hardness allow it to overcome the last two disadvantages. Furthermore, 4H-SiC wafers with defect densities lower than diamond are now available in sizes up to six inches in diameter [37]. However, in order to be used in transmissive mode, devices must be thinner than 10 μm in order to achieve X-ray transmission greater than 90% for photon energies greater than 10 keV [91]. As we saw in paragraph 3.1.2, a new technique, electrochemical etching in HF-based solutions, has only recently been developed, enabling the fabrication of SiC membranes with thicknesses of $< 1\mu m$ [36].

Using an 8 keV X-ray beam at PSI in Switzerland, Nida et al. [37] investigated the performance of a 1.6 μm 4H-SiC p–n junction with micrometre n-type thin active epitaxial layers. Results are compared with performance of a 12 μm commercial polycrystalline diamond, which is the solid state detector of choice for this application due to its excellent transparency, radiation hardness, and thermal conductivity. Beam transmission as a function of beam lateral position is measured to be > 95%, which is compatible with that of the diamond within error bars. At zero bias, the 4H-SiC has a charge collection efficiency of 100%. In addition, the response of the 4H-SiC XBPM to variations in photon flux is investigated for 12.4 keV photons in the flux range ~ $0.01 - 1000 \cdot 10^9\, ph$/sec. The 4H-SiC XBPM shows a much faster dynamics (in the microsecond range) compared with pc-diamond (millisecond range). Furthermore, in terms of linearity, the response to photon flux is similar to that of a silicon diode, i.e. it is linear over a four-order-of-magnitude range.

4.3.2.4 Dosimetry

Another interesting application for SiC-based sensors as X-ray detectors that has been investigated in the past is their potential use as dosimeters. Indeed, SiC has a better Z match to tissue properties than Si diodes (the primary semiconductor devices used as *in vivo* dosimeters), in addition to the well-known advantages SiC has over Si diodes (Section 2). In Ref. [89], the feasibility of SiC-based dosimeters was investigated using 6 MV brehmstrahulng photons from a 6-MeV electron beam. The current response was measured vs. photon dose rate in the 2–7 Gy/min range, which is a dose rate of interest in radiotherapy. With a slope of $3.5 \cdot 10^{-10} A \cdot \text{min}/Gy$, the sample polarized at 150 V exhibits high linearity, with the released charge increasing with the photon dose. A SiC Schottky diode was also tested as a dosimeter in Ref. [90] using 6 MV bremsstrahlung photon beams from a 6 MeV electron beam. The SiC at zero bias was used to measure the collected charge vs. radiation dose. Results are compared to that obtained with three standard commercially available silicon dosimeters. A linear, stable and reproducible response was observed with very low leakage currents even after the irradiation (of the order of pA/cm of current density at room temperature). The sensitivity of the

TABLE 4 A list of some works cited in Par. 4.4 with related detector properties.

Ref	Det. type	Doping [cm^{-3}]	Thickness	Area [mm^2]
[107]	Schottky	n/a	100 μm	28.3, circular
[108]	n/a	n/a	n/a	n/a
[104]	p-n	$2 \cdot 10^{14}$	20 μm	33, circular
[105]	p-n	$5.4 \cdot 10^{14}$	20.9 μm	2.13, circular
[106]	p-n	$2 \cdot 10^{14}$	20 μm	33, circular
[109]	Schottky	$5 \cdot 10^{14}$	50 μm	from 4 to 20
[97]	Schottky	$4.7–9.1 \cdot 10^{14}$	25–270 μm	1×1

Doping and thickness refer to the epitaxial layer.

4H-SiC dosimeter was 23 nC/Gy, i.e. comparable to those of commercial silicon dosimeters.

4.4 Neutron detection

Neutrons do not interact with valence electrons and then their detection is demanded to reaction products, like γ-rays, tritons, alpha and heavier ions. A neutron detector's most important parameters are sensitivity and linearity. Low operation bias and γ discrimination are two advantages of semiconductor detectors over ^3He, whose availability on Earth is also limited.

SiC is an intriguing material for the fabrication of neutron detectors due to its properties. It is not the only one, either. Diamond neutron detectors were made possible by recent advances in CVD technique [92–95].

Several factors influence the sensitivity of neutron SiC detectors, including the concentration of deep carrier traps during growth, the type and thickness of the conversion layer (discussed below), and the charge collection active volume (larger volumes are in principle better but they mean bigger capacitances that are detrimental for the noise).

SiC neutron detectors were reviewed by Franceschini and Ruddy in 2011 [96], Coutinho et al. in 2020 [97] and Ruddy et al. in 2021 [98], the latter with a specific focus on their use in harsh nuclear environments.

A list of works cited in this Paragraph is reported in Table 4, along with related detector properties.

From the several studies conducted on SiC neutron detectors the following conclusions can be extracted:

- SiC detectors have a linear response to thermal [99, 100], epithermal [101, 102], fast [103] and 14-MeV neutrons [102].
- Energy resolution of ~ 3% has been observed for the $^{12}C(n,\alpha)^9Be$ related-peak at ~ 9 MeV [104].
- Neutron detection at high temperature show interesting results. For example, a temperature of 500°C does not significantly affect the peak position and the energy resolution of the $^{12}C(n,\alpha)^9Be$ related peak [105].
- 100% neutron-gamma discrimination has been observed [106].
- A sensitivity of $10^{-5} counts/(n/cm^2)$ for thermal neutrons has been reported [97].

To describe the possible processes of a neutron impinging on a SiC detector, as well as the different SiC detector structures involved in neutron detection, two energy regimes can be considered separately: fast neutrons ($E_n \gtrsim 10$ MeV) and thermal neutrons ($E_n \sim k_B T$ at room temperature).

4.4.1 Fast neutrons

The most likely interactions for a fast neutron crossing a SiC detector are elastic and inelastic scattering $^{12}C(n,n')^{12}C$. C and Si nuclei can be removed from their sites depending on the amount of energy transferred in the collision, and the event can then be observed as a permanent point defect or by collecting the e-h pairs created by the recoil atom in the depleted region. Other reactions that may occur with a lower probability include $^{12}C(n, n')3\alpha$, $^{28}Si(n,p)^{28}Al$, $(n, 2n)$, (n, pn), $(n, n\alpha)$, or reactions involving the detector's less abundant C and Si isotopes [110].

4.4.1.1 Fission neutrons

The presence of energetic ^{12}C and ^{28}Si ions from elastic and inelastic scattering dominate the energy spectrum produced in a SiC detector for fission neutrons, i.e. neutrons with energies less than 6 MeV (most of them) and average energy of about 2 MeV. The spectrum is generally complex, with no peaks. As a result, information must be extracted through the unfolding of the spectrum using neutron transport codes and range calculations for recoil nuclei [96].

Wu et al. [108] investigated the performance of 4H-SiC detectors for fission neutron measurements. They demonstrated that increasing the thickness of the epitaxial layer from 20 to 120 μm improves sensitivity to neutron pulses by 139.8%. Using the proton-recoil method, an additional 11.6% increase is obtained.

4.4.1.2 Mono-energetic neutrons

A different situation is when monoenergetic fast neutrons impinge on a SiC detector, like for example 14 MeV neutrons from a Deuterium-Tritium (DT) neutron generator [98]. The continuum contribution from elastic and inelastic scatteing on Si and C dominates the spectrum at low energies, but defined peaks appear as well. As reported in Ref. [98], the detection of the $^{12}C(n,\alpha)^9Be$ reaction products yielded a peak at 8.298 MeV, as well as some peaks from the $^{28}Si(n,\alpha)^{25}Mg$ reaction corresponding to different levels of the ^{25}Mg, which dominated the high energy region of the spectrum.

A fast-neutron SiC detector can gain sensitivity by adding a layer of converter material in front of it, which is rich in nuclei

with large scattering cross-sections for fast neutrons, which can produce e-h pairs within the depletion region after they recoil. Fast neutrons have a large scattering reaction cross-section with hydrogen, and the latter has a large penetration depth into the semiconductor, so materials with a high density of hydrogen, such as polyethylene, have two advantages. One disadvantage is that such materials are difficult to withstand high temperatures and radiation levels.

Flamming et al. [107] use a polyethylene converter in front of a SiC detector to detect 2.5 MeV neutrons from a deuterium-deuterium (D-D) neutron generator. Sensitivity to proton recoil increases by increasing the thicknesses of the polyethylene layer up to 100 μm, a value basically corresponding to the range of protons in the converter. As expected, increasing the incidence angle of a neutron on the detector surface reduces sensitivity (about half at 45° with respect to perpendicular direction). This effect is due to the lower $^{1}H(n, p)n$ cross-section and lower p recoil energies for larger scattering angles. In theory, this "directionality" of the response could be used to extract information on neutron source spatial distribution, location, and distribution. Two features that are particularly useful in the field of nuclear reactor fuel characterization and the detection of hidden fissionable materials.

The response of SiC and diamond for the detection of 14 MeV neutrons at a fluence rate of about $9.4 \cdot 10^{6} cm^{-2} \cdot s^{-1}$ is compared in Ref. [104]. The p-n junction is formed by deposition on the epitaxial layer of a 11 μm-thick p^{+} layer characterized by an aluminum doping concentration as high as ~ $10^{19} cm^{-3}$. In both detectors the peak due to the $^{12}C(n,\alpha)^{9}Be$ reaction is observed with a slightly better resolution in the SiC (260 keV at FWHM corresponding to ~ 3.1%), with respect to 303 keV ~ 3.6% observed in the diamond detector. The count rate is strongly influenced by the active volume of the detector, which is why it was found to be higher in this study in the diamond-based detector.

4.4.1.3 High temperature measurements

Still in the field of fast-neutron detection, Szalkai et al. [105] report on several tests on SiC detectors performed with 14 MeV neutrons at various temperatures. The behavior of SiC devices at high temperatures is fascinating because of their potential applications in fields such as reactor monitoring, where neutrons and charged particles must be reliably detected at high temperatures. As we will *see* in Paragraph 5.3, it has significant implications for radiation damage. The structure of the detector used is the following: on a 350 μm thick n^{+}-type 4H-SiC substrate a 0.5 μm thick buffer n-epitaxial SiC layer ($10^{18} cm^{-3}$) was grown; on the top of the buffer layer, a 20.9 μm thick n-type epitaxial ($5.4 \cdot 10^{14} cm^{-3}$) layer was deposited. To create the pn-junction a $10^{19} cm^{-3}$ Al-doped, ~ 1 μm thick p^{+} layer was then placed above; to create a high temperature resistant metallic contact, a 300 nm thick nickel layer was grown on the p^{+} layer with 250 nm thick gold over-metallization. The surface of the diode was 2.13 mm^{2}. Due to the described doping structure, 220 V are required for a complete depletion of the epitaxial layer. The most prominent structure in the measured energy spectra, namely the $^{12}C(n,\alpha)^{9}Be$ reaction peak, is clearly visible up to 500°C, with no change in peak position (9.09 MeV) and only a slight broadening in the energy resolution (FWHM = 0.22 MeV at T_{room} and 0.25 MeV at 500°C). A decrease in the counting rate, from ~130 at T_{room} down to ~ 60 counts/sec at 500°C is observed. It is recommended that operating voltages be reduced at high temperatures to prevent the detector from deteriorating due to increased thermal noise. Finally, epitaxial Silicon Carbide lacks polarization effects due to temperature increase [98], which are present in diamonds starting at 327°C [111]. A polarization effect is the interference between charge carriers and transient space-charge fields generated by trapping/detrapping events in defects [97].

4.4.2 Thermal neutrons

A converter layer is required to detect thermal neutrons, and the sensitivity of the detector is largely determined by its properties. The coverter can be applied as a thin layer in front of the SiC sensor, or it can be directly incorporated using diffusion [112] or ion implantation [113]. This layer must be rich in isotopes with large cross-sections for thermal neutrons, such as ^{6}Li, ^{10}B, or ^{235}U. To report some numbers, assuming a 0.0253 eV neutron, the absorption cross sections of ^{28}Si and ^{12}C are 0.17 and 0.00353 b, respectively, much lower than 681, 938, and 3843 b for ^{235}U, ^{6}Li and ^{10}B. Aside from the cross-section, the penetration depth of the reaction products into the depleted layer is another important parameter that influences the detector response is the reaction of interest for ^{6}Li, with E_{α} = 2.05 MeV and E_{t} = 2.73 MeV. The presence of ^{4}He and ^{3}H events dominates the detector response over the above discussed fast-neutron induced reactions when a ^{6}LiF converter foil is used. One α at 1.47 MeV and one ^{7}Li at 0.84 MeV are emitted in the $^{10}B(n,\alpha)^{7}Li$ reaction. Thus, due to the higher penetration depth of the tritons, the ^{6}Li reaction products have the potential to be more efficient in the generation of electron-hole pairs than the ^{10}B reaction products, despite the fact that the ^{6}Li cross-section is significantly smaller than the ^{10}B cross-section.

SiC diodes used as thermal neutron detectors have shown general features. The type and thickness (or concentration) of the conversion layer, which influence the amount of energy released by a neutron event in the active region of the detector, essentially determine sensitivity to thermal neutrons. In this way, by properly tuning the reverse bias, the neutron signal can be better distinguished from possible accompanying gamma and X-ray radiation. In SiC detectors, 100% neutron-gamma discrimination and linear response to the neutron flux have been reported in Ref. [106].

It has been also observed that at fluences greater than $10^{13} n/cm^{2}$, the produced fission fragments can damage the device and reduce the counting rate [97].

Refs. [106, 109] provide a comparison of SiC and diamonds for the detection of thermal neutrons. Diamonds, in theory, are more radiation-resistant than SiC because of their larger atomic displacement energy (40–50 eV for Diamond, 20–35 eV for SiC). Diamonds, on the other hand, can exhibit polarization effects, as mentioned in the previous paragraph. This is also true in cases where high neutron fluxes, such as those above $10^9 n/(cm^2 \cdot s)$, result in a high defect density [106].

Coutinho et al. [97] present a review of the use of SiC neutron detectors, with a focus on social applications such as the prevention of illicit radiological material trafficking through cargo screening. The operating bias of the detector in their study was between 50 and 100 V. Detectors have been tested at the JSI TRIGA reactor (Ljubljana, Slovenia). At maximum reactor power (250 kW), neutron fluxes of up to $1.6 \cdot 10^7 n/cm^2 s$ have been used. Conversion layers consisting of ^{10}B and ^6LiF-enriched powders deposited onto a plastic film mounted at a distance of about 2 mm from the SiC surface were used in the detectors. Regardless of epilayer thickness or converter type, the detectors showed excellent linearity (counting rate vs. reactor power). On average a sensitivity of $10^{-5}(counts/s)/(n/cm^2 s)$ is found with better performances with ^6LiF layers. Further optimized SiC detectors could potentially begin to compete with BF_3 and ^3He detector detector sensitivities [97, 114].

4.5 SiC for laser-generated plasma radiation

Laser-generated beams have unique properties that necessitate the development and application of dedicated beam diagnostic detectors. Short pulses (0.1–1 ns), high peak currents (10^{10} to 10^{12} proton/pulse), very high dose rates ($10^9 Gy$/min), and the presence of a mixed radiation field per single pulse shot (visible radiation, UV, X-rays, electrons, protons, and, eventually, ions) [115]. The use of large-bandgap semiconductor detectors, such as SiC, allows for a reduction in the low-energy electromagnetic spectrum, improving proton/ion sensitivity. Diamond and silicon carbide detectors, for example, have low capacitance, radiation hardness, and time/energy resolutions that make them suitable for time of flight (TOF) measurements of high-energy laser-driven beams.

V. Scuderi et al. [115] conducted a thorough investigation of the performance of diamond and SiC detectors as diagnostic systems for the ELIMAIA (ELI Multidisciplinary Applications of Laser-Ion Acceleration) beamline at the ELI-Beamlines research center in the Czech Republic. V. Scuderi et al performed a sophisticated analysis based on deconvolution of the ToF signal produced by the cocktail beam to extract the accelerated species' energy cut-offs, energy distribution, and fluence.

A 21 μm thick $2 \times 2\ mm^2$ SiC was placed along the beam direction at 106 cm from the target (a pure cryogenic hydrogen target) in Ref. [74] to detect protons generated by a 2 TW PALS laser in Prague (600 J energy and 300 ps time pulse). The detector operated at 150 V corresponding to a depleted region of 5 μm. A mixture of protons with different emission energies appears in the Volt vs. ToF signal measured during one laser shot. In the 450 KeV–1 MeV range, five different proton populations have been observed. A rise time of 3 ns was measured, demonstrating how SiC detectors and the TOF method can be used to diagnose plasma-accelerated beams.

In Ref. [116] a 4H-SiC detector was used, with an 80 μm thick undoped epitaxial layer grown on an n-type doped active layer. The SiC was biased at 400 V and placed at 10° in the backward position. The detected current signal was sent directly to a 500 MHz oscilloscope's 50Ω impedance. Although the photopeak is not completely cut, the measured current vs. ToF signal for a laser energy of 600 J (at PALS, Check Republic) and a Si target, shows high sensitivity to fast protons and low responsiveness to UV radiation.

In another measurement at PALS, [75] used a circular 4H-SiC detector with a 5 mm^2 area and a 115 μm thick epitaxial layer, unintentionally doped at $5 \times 10^{13} cm^{-3}$, and 250 V applied to the ohmic contact, resulting in an active region 72 μm thick. In this case, the sensor was also positioned in the backward direction at 15°. Through the 50Ω load resistance of a 1 GHz, 5 GS/s oscilloscope, currents up to 1.6 A were measured and converted into voltage signals (up to 80 V). The authors observed a high signal-to-noise ratio, nanosecond time resolution, and no degradation of the detector performance from different Voltage vs. ToF signals measured at laser energies of 520 J and with different targets.

4.6 SiC for beam-monitoring and dosimetry in flash radiotherapy

In the last few years, investigation of innovative radiotherapy strategies has driven the development of novel technologies for radiation dosimetry and beam monitoring. In particular, the increasing interest towards the so-called "FLASH radiotherapy," which makes use of ultra-high dose-rate (UHDR) beams for better preserving healthy tissues surrounding the tumor target, is paving the way for the establishment of alternative radiation detection approaches. Indeed, the response of currently used active detectors for dosimetry and beam monitoring, such as ionization chambers, is strongly affected at these regimes, which are characterized by dose rates at least three order of magnitudes larger than the ones used for conventional radiotherapy. Solid state detectors have been recently investigated, as a valuable alternative for real-time measurements. In particular, silicon Carbide (SiC) detectors were never systematically tested in the past at these regimes.

Recently, the response of novel ultra-thin SiC detectors with thickness between a few μm and 20 μm was experimentally

characterized with low energy UHDR electron beams (7 and 9 MeV) accelerated by a LINAC designed for FLASH-RT studies (SIT-Sordina ElectronFlash accelerator). First promising results have been obtained in view of possible beam monitoring and dosimetry of UHDR beams for FLASH radio-therapy applications [117]. The device structures used is made of a thin, highly doped p^+ layer ($10^{19}cm^{-3}$, 0.3 μm), a n^- low doped layer (either 10 μm or 2μm, $8 \cdot 10^{13}cm^{-3}$) on top of a n^+ thick substrate (370μm, $5 \cdot 10^{18}cm^{-3}$). In their ultra-thin version, i.e. as "free-standing membrane," the n^+ thick substrate can be selectively removed by means of electrochemical etching (Par. 3.1.2). Doses per pulse up to 10 Gy were delivered with a pulse duration of 2 s. Results show a linear trend of the detector response up the several Gy/pulse. Radiation damage measurements were also carried out up to several hundreds of kGy, for which the response of SiC was found stable. New geometrical configurations (strip) are being developed and tested by the same Authors with the aim of providing accurate dose rate independent 2D beam monitoring measurements. Moreover, pixelated version are also under construction with the potential to be used for relative dosimetry thanks to their high spatial resolution (of the order of tens μm).

4.7 SiC for sub-GeV dark matter

The tiny nuclear recoil energy involved in direct searches for non-relativistic sub-GeV Dark Matter poses a significant challenge. This problem is currently being addressed in two ways. The detection of recoil electrons is one strategy, while the use of light nuclei, such as those found in SiC, is another. In a recent work Griffin et al. [118] proposed for the first time the use of SiC for direct detection of sub-GeV dark matter. As the authors point out, SiC has some distinct advantages over Diamond and Si in this research field. To probe a significant portion of the DM parameter space in a reasonable amount of time, O(years), detector masses in the kilogram range are required. Large SiC wafers can be made with current technology, but single diamond crystals of significant mass are difficult to come by.

The authors performed detailed calculations on the potential sensitivity of SiC targets for various types of DM while taking into account the possibility of collecting charge or heat from SiC. In terms of the latter, SiC is a promising candidate for phonon readout due to its high sound speed and long intrinsic phonon lifetime (which is longer for politypes with smaller unit cells). The reach calculated by the authors for both DM-nucleon and DM-phonon interactions is unaffected by the SiC polytype used. The DM-electron scattering channel is dependent on the polytype, changing the potential reach, due to differences in band-gap (Paraghraph 2.2) between the politypes; better sensitivities are found for smaller bandgap and larger unit cell of H politypes. The authors examine the properties of various politypes also in the context of potential directional searches. They notice that 2H-SiC, which has an anisotropic response due to the different in-plane and out-plane crystallographic axes, achieves the highest daily modulation. The symmetric 3C cubic phase, on the other hand, is expected to have no modulation. Aside from the possibility of directional searches, the authors suggest SiC as a potentially excellent detector over a wide range of DM mass ranges, depending on the scattering channel: DM-nucleon down to O(10 keV), DM-electron down to O(10 MeV), dark photon and axionlike absorption down to O(10 meV).

5 Radiation hardness studies

Irradiation of the detectors can produce faults in addition to the as-grown defects discussed in Par. 3.1.4. Bulk damages can be caused by the non-ionizing energy loss of energetic particles such γ-rays, neutrons, electrons, protons, alphas, and heavy ions. To remove a C or a Si from their lattice position, energy greater than 21 eV and 35 eV is required, respectively. When a lattice atom is pushed away from its equilibrium position, vacancies and interstitial atoms can form. These are the so-called primary radiation defects. The majority of these primary defects recombine, whereas the others form deep levels in the energy gap. In general, increasing the device temperature can anneal out a certain number of primary defects, but some of them may interact with each other and impurity atoms, resulting in secondary radiation defects. Bulk damages refer to both primary and secondary faults of this nature. At high fluences, ionizing radiation loss can change the inter-electrode capacitance (surface damage) and impact the breakdown characteristics and electronic noise.

Silicon vacancy (V_{Si}) [119], carbon interstitials(C_i) [120], and carbon antisite-carbon vacancy (CAV) complex [121] are the most dominant radiation-generated defects in SiC [9]. The two electrically active defects S1 and S2, produced by epithermal and rapid neutron irradiation and appearing at about 210°K and 350°K in the DLST spectrum, respectively, are examples of V_{Si} [9].

As the absorbed radiation dose rises, so does the amount of generated defects, lowering SiC detector performance. Bulk damages, whether in the form of point defects or clusters, are responsible for the following: a decrease in signal amplitude due to charge carrier trapping; a rise in ohmic resistance due to a decrease in free carrier concentration; a shortening of carrier lifetime and diffusion length due to an increase in the concentration of recombination centers; an increase in the leakage current due to the formation of charge-donor states; and a change of effective doping concentration.

The effects of radiation on SiC detectors have been thoroughly studied [122–125]. A comprehensive review of the topic for various radiations can be found in Ref. [5]. The majority

of published papers, such as [18, 60, 126–128], focus on Schottky structures, while others, such as [59, 129, 130] on pn junction diodes. The following paragraphs group the findings of irradiation investigations by irradiation type.

5.1 Irradiation with electrons, protons, and heavy ions

A significant amount of work has been published on the subject. Radiation damage is strongly dependent on the device structure and radiation type/energy, thus a tentative to summarize and find some general conclusion is hard. Nevertheless an attempt to ouline some general features is reported in the following:

- Electron and proton-produced defects have similar structures and capture cross sections.
- Electron and proton irradiation starts to significantly degrade the CCE and the electric rectifying properties of SiC at around 10^{14}–$10^{15} cm^{-2}$. Some detector have been reported to work, altghogh with degraded perfoemances, even at electron and proton fluences of ~ 10^{16} [5, 91].
- Low energy (35 MeV) ion irradiation (^{16}O) at fluences of ~ $5 \cdot 10^{15} cm^{-2}$ degrades the CCE and the energy resolution by a factor of 2 and 10, respectively [13].
- Irradiation at high temperatures are beneficial in both electrons and protons irradiaion [131].

Many studies have been carried out on the effects of protons irradiation over a wide range of energies and fluencies, namely from 6.5 MeV to 24 GeV and from 10^{11} to $1.4 \cdot 10^{16} p/cm^2$ [5].

One of the first pieces of evidence discovered was that the proton's energy has a minor impact on the structure of the defect created [132, 133]. On the other hand, it determines the rate at which the deepest induced defects are introduced (defect-concentration/radiation-fluence). Indeed, the scattering cross section of protons on Si and C decreases as proton energy increases, resulting in a lower introduction rate. Aside from incident energy, radiation fluence is, of course, an important factor in radiation damage. Deep-level concentration, removal charge rate, and L_p are all strongly influenced by proton fluence. This is especially true in the case of the CCE. For both the polytypes 6H–SiC and 4H–SiC, it was discovered that increasing the proton fluence increases the deep-level concentration and rate of removed charge carriers, while decreasing the minority charge carrier diffusion length and CCE [134].

As summarized in Ref. [5], DLTS measurements indicate that, even at very different energies (6.5 MeV at $3.2 \cdot 10^{13} p/cm^2$ [135], 8 MeV at $2 \cdot 10^{16} p/cm^2$ [133], and 24 GeV at $1.4 \cdot 10^{16} p/cm^2$ [127]) the main effect in the electrical behaviour of SiC Shottcky diodes is due to a level (identified with the R center) located at 1.1–1.2 eV below the conduction band and charachterized by a high capture cross section of $2 - -5 \cdot 10^{-13} cm^2$ [133, 135].

The results of irradiating 4H–SiC epitaxial diodes with 24 GeV protons are reported in Ref. [5]. With 2.3 MeV beta particles from a ^{90}Sr source, the CCE as a function of reverse bias has been measured in particular. Sensors that have not been irradiated have a CCE of 100%. Diodes were still able to detect beta particles after irradiation at very high fluences of $1.4 \cdot 10^{16} pcm^{-2}$, though with a low response, i.e. a CCE between 10 and 25% for a reverse bias around 250 and 700 V, respectively.

Irradiation temperature has recently been shown to play a significant role in the radiation resistance of SiC detectors. According to Lebedev et al. [131], as the detector temperature rises during irradiation, not only are deep acceptor levels partially annealed out, but their formation probability decreases as well.

Rafi et al. [91] recently investigated the effects of electron and proton irradiation on four-quadrant pn junction diodes made on epitaxial 4H-SiC substrates with a 30 μm thick n-type epilayer doped at $1.5 \times 10^{15} cm^{-3}$. Fluences as high as $1 \times 10^{16} e/cm^2$ and $2.5 \cdot 10^{15} p/cm^2$ have been studied. A ^{239}Pu –^{241}Am –^{244}Cm tri-α source is used to investigate the device's performance as a radiation detector. At room temperature, the investigated SiC sensors can work as radiation detectors up to the highest fluences. However, starting at $1 \times 10^{15} e/cm^2$ the loss of the electrical rectification character of the devices can be seen in the I-V and C-V electrical characteristics. Leakage currents measured at 400 V are on the order of 1 nA, regardless of the absorbed dose. There are no significant differences between proton and electron irradiation, confirming that electron and proton-produced defects have similar structures and capture cross sections [5]. Around 250 V, CCE reaches saturation. For fluences greater than $1 \cdot 10^{16} e/cm^2$, a non-negligible CCE reduction of about 10% is observed.

SiC detector performances were tested in terms of CCE in Ref. [136] using ^{241}Am-generated α and 8.2 MeV electron irradiation at $4.74 \cdot 10^{13} e/cm^2$ (2 Mrad), $2.37 \cdot 10^{14} e/cm^2$ (10 Mrad), $4.74 \cdot 10^{14} e/cm^2$ (20 Mrad) and $9.48 \cdot 10^{14} e/cm^2$ (40 Mrad). CCE is rapidly degraded at 2 Mrad and continues to degrade at a slower rate at higher doses. The use of reverse bias $\geq 200V$, on the other hand, ensures 100% CCE even at the highest dose.

Many other studies have been carried out on the effects of electrons irradiation on SiC, as for example [137–143]. Defects concentration, formation rates, energies, and capture cross sections of defects created by electrons with energies ranging from 1.7 to 4 MeV have also been extensively studied [122, 144–148].

Sciuto et al. [149] irradiated 4H-SiC n-type epitaxial p-n junction UV detectors fabricated by Al implantation with α particles at very low energy (600 keV). A wide range of fluences ($5 \cdot 10^{11}$–$5 \cdot 10^{14} ions/cm^2$, i.e. from a few kGy to a few MGy dose) has been investigated. Optical measurements confirmed the photodiodes' visible blindness even after irradiation. The optical responsivity drops to ~ 50% for fluences of $< 10^{13} ions/cm^2$ (~90 kGy), but dark current values

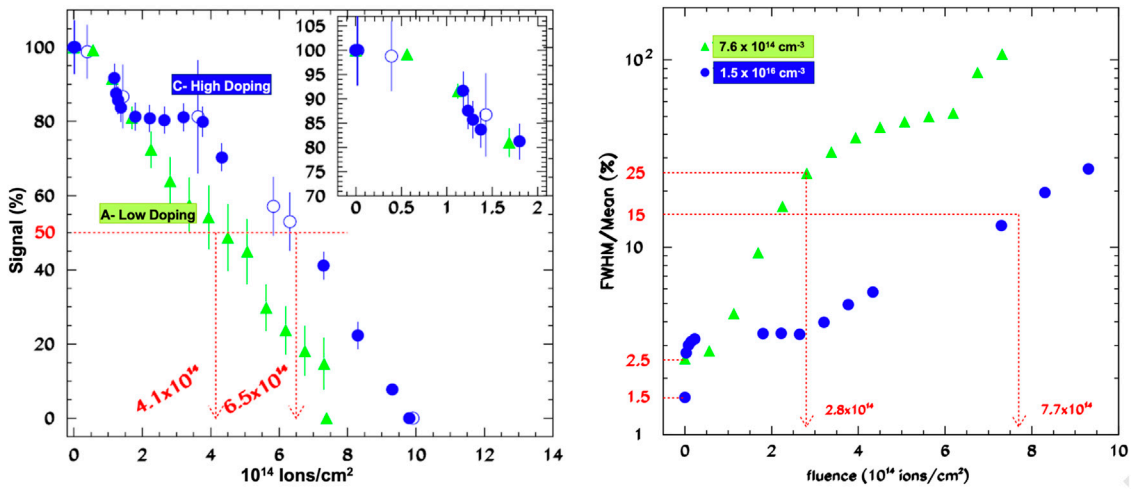

FIGURE 7
Left: Percentage of the signal generated by ^{16}O ions after irradiation as a function of the ion fluence. Two SiC detectors with different doping concentrations are compared. SiC have been irradiated with ^{16}O ions at 32.7 MeV. Right: Variation of the two SiC detectors' energy resolution as a function of irradiation fluence. Data are from Ref. [58].

remain stable. Photo-detection capabilities are severely hampered by the formation of complex defecs at higher fluences.

De Napoli et al. [58] irradiated 4H-SiC detectors with ^{16}O ions at 35.2 MeV to investigate the radiation resistance of SiC detectors to ions and possible dependencies on doping concentrations. In particular, two SiC detectors with doping concentrations of $7.6 \cdot 10^{14}$ and $1.5 \cdot 10^{16} cm^{-3}$ were used. The depleted epitaxial regions were 32.7 and 9.2 μm with a bias of 600 and 400 V, respectively. The fraction of ^{16}O signal observed after irradiation as a function of accumulated ion fluence is shown in Figure 7 - left panel. Charge collection became increasingly inefficient as the latter was increased, shifting the ^{16}O energy peak to lower values. At fluences of $6.5 \cdot 10^{14} ions/cm^2$ and $4.1 \cdot 10^{14} ions/cm^2$ for the heavier and lower doped SiC, respectively, CCE is reduced to half its non-irradiated value.

Due to an increase in collected charge fluctuations, also the energy resolution deteriorates with increasing absorbed doses (Figure 7 - right panel). The lighter doped SiC shows again the worst performance. Its resolution becomes a factor 10 worst with respect to the non-irradiated detector resolution at a fluence of $2.8 \cdot 10^{14} ions/cm^2$. The same result is observed in the heavier doped SiC at the higher fluence of $7.7 \cdot 10^{14} ions/cm^2$.

Finally, in Ref. [150], studies on SiC Schottky irradiation with heavier ions (Xe, Kr, Ar, Ne, and N) show that leakage currents increase linearly as a function of the number of incident ions.

5.2 Irradiation with x-/γ-rays

Because their energies are lower than the Si and C dislocation energies reported at the beginning of this Section, x-rays cannot cause bulk damage. Nevertheless, SiC detector performance can degrade at high radiation doses, such as 1 Mrad/s or higher, due to interface traps [151] and traps created in the dielectric materials used for isolation and passivation [91].

Many studies on radiation hardness against γ, primarily gammas from nuclear sources, have been published. Some general conclusion can be drown:

- If irradiated with γs, SiC detectors can be classified as radiation hard. When compared to charged particles and fast neutrons, the effects of γ-rays on detector response are minor.
- Even after very high doses (up to 27.72 MGy), high CCE values (> 80%) can be achieved if a high enough over bias is applied.
- In general, the type of metal electrode determines the irradiation-induced increase in leakage current. A detector with a Ti/Au electrode deposited on the SiC sensor, for example, showed a fluctuation of only ~ $100nA$ at 100 V after 5.14 MGy irradiation.

Nava et al. [122] found that after γ irradiation from a ^{60}Co source up to 5.4 MGy, the CCE of SiC detectors remains 100% if a high enough reverse bias is applied.

Ruddy et al. [125, 152] investigated the performance of SiC Schottky diodes under intense γ irradiation in two papers. They measured the ^{238}Pu α response of a 4H–SiC Schottky diode after exposure to ^{137}Cs γ-rays. Though energy resolution and peak position slightly decrease, spectrometry performance is maintained up to 5.4 MGy with a CCE of 100%. Even at a massive dose of 27.72 MGy, the detector continues to work

with a CCE of 84%. However, these results are obtained at a bias voltage of −600 V which is significantly higher than the operating bias (−100 V) of non-irradiated SiC.

In Ref. [153], the role of the metal electrode on the radiation tolerance of gamma-irradiated SiC was investigated. With electrode structures of Cr/Au, Ni/Au, and Ti/Au (Cr, Ni, or Ti of 30 nm thickness deposited by sputtering, plus 200 μm Au deposited by the thermal evaporator), three detectors were used. The detectors were exposed to γ-rays from ^{60}Co at doses of 2.7, 5.4, and 8.1 MGy, respectively. The detectors equipped with the Ti/Au electrode show the lowest increase in leakage current, from 0.18 to 0.31 μA at 100 V, while those equipped with the Ni/Au electrode show the highest increase, with a value of 0.24 μA, which is a factor 15 higher than the pre-irradiation value. The CCE measured with ^{238}Pu generated αs after 8.1 MGy irradiation still reached 100%, but for a reverse bias about four times higher (about 160 V) than that required before irradiation, regardless of the electrode type [153].

The effects of γ-ray irradiation into 6H-SiC diodes has been also investigated several times. Different groups used ^{60}Co γ-ray source exposing the detectors at large doses: at 120 kGy even a decrease in the leakage current has been observed [124], at 1.080 MGy the γ-ray detection efficiency of SiC photodiodes has been observed to not change [154], and at 2.5 MGy a charge collection efficiency of 100% in p-n SiC diodes has been measured [155].

5.3 Neutron irradiation

Neutrons, as well as the charged particles produced in the converter layer, can cause damage. The latter appears to be more severe than γ damage in SiC detectorts. Several different studies have been conducted by various groups. Ruddy et al. [98] recently published a review on the subject. Some of the findings can be summed up as follows:

- In general, at fluences of the order of $10^{11} n/cm^2$, SiC detector performance begins to deteriorate due to epithermal/fast neutron irradiation [97, 156]. However, no significant CCE degradation is expected. Radiation effects become important at fluences greater than about 10^{14}–$10^{15} n/cm^2$, resulting in an acute degradation of the CCE and a reduction in e and h drift length. However, even after a fluence of $1.7 \times 10^{17} n/cm^2$ some detectors have been found to still work [5].
- Cases where SiC becomes semi-insulating at fluences of $4 \cdot 10^{14} n/cm^2$ have been reported [5]. The effect is caused by electrons being trapped in radiation-induced deep level defects.
- SiC UV-photodiodes with drift layer doped less than $1 \times 10^{15} cm^{-3}$ preserve their performance up to fluence of $5 \times 10^{12} (fast - neutrons)/cm^2$.
- Elevated temperatures during irradiation attenuate the effects of the radiation damage on CCE, opening the possibility of using SiC neutron detectors in high-temperature environments.

Seshadri et al. [157] performed fast neutron (E > 1 MeV) irradiation studies on 4H-SiC Schottky diodes. The charge collection efficiency of ^{238}Pu was found to degrade in a systematic manner due to neutron damage-induced defects. In particular, radiation-induced deep-level traps remove carriers at a rate of $9.7 \pm 0.7\ cm^{-1}$ until the self-biased operation is prevented at an accumulated fluence of $5.7 \times 10^{16} cm^{-2}$.

Radiation damage due to fast neutrons has been also studied by Dullo et al. [99, 100], on 4H-SiC Schottky diodes used as thermal neutron detectors with a ^6LiF converter layer. Between the converter and the detector, an Al foil was placed to stop neutron-induced alpha particles ($^6Li\,(n,\alpha)^3H$) and thus minimize radiation damage. At fluence rates ranging from 1.76×10^4 to 3.59, $\times$, $10^{10} cm^{-2} s^{-1}$, the neutron response was found linear within 5% of uncertainty. No variations have been observed after irradiation with fast-neutron ($E > 1\ MeV$) at a fluence of $1.3 \times 10^{16} cm^{-2}$.

Moscatelli et al. [59], irradiated SiC p^+n diodes with 1 MeV neutrons in the range 10^{14}–$10^{16} n/cm^2$. They measured the CCE as a function of neutron fluence using electrons from a ^{90}Sr source. The CCE decreases as the fluece increases, remaining very high only until some $10^{14} n/cm^2$.

Wu et al. [128] studied the CCE for 3.5 MeV alpha particles from a ^{241}Am source in self-biased (i.e. zero external bias) 4H-SiC Schottky diode irradiated with fast neutrons. They found that the CCE decreases by increasing the neutron fluence, reaching 1.3% after an irradiation at $8.26 \times 10^{14} n/cm^2$.

Nava et al. [158], report results on radiation resistance of 4H-SiC detectors irradiated with 1 MeV neutrons up to a fluence of $8 \times 10^{15} n/cm^2$. As expected, increasing the neutron fluence causes the CCE to decrease, but at two different rates. The CCE decreases monotonically by about 30% in the first regime, from 10^{13} to $10^{15} n/cm^2$. CCE drops from 70% to 20% in the second one, from 10^{15} to about $10^{16} n/cm^2$. Two deep levels were found using Photo Induced Current Transient Spectroscopy (PICTS), one at 1.18 eV associated with a carbon vacancy and the other at 1.5 eV associated with a complex defect of C and Si vacancies. They are cited by the authors as the source of the CCE reduction.

Higher-energy neutrons (14 MeV) from deuterium-tritium fusion were used to irradiate SiC detectors with Schottky diode structures in Ref. [126]. The sensitive volume of detectors is $1mm \times 5\ mm \times 20\ \mu m$. The 20 μm thick epitaxial layer, doped at $10^{14} cm^{-3}$, is growth by CVD onto 350 μm thick substrate doped at $10^{19} cm^{-3}$. Detectors have been irradiated at room temperature. At 300 V, the CCE measured with alpha from a ^{239}Pu source decreased by about 7.0% and 22.5% at fluences of $1.31 \cdot 10^{14} n/cm^2$ and $7.29 \cdot 10^{14} n/cm^2$, respectively. Despite this CCE reduction, SiC diodes can still be used as raditaion detectors.

4H-SiC UV-photodetectors were irradiated with 1 MeV neutrons at various fluences ranging from $5 \times 10^{12} cm^{-2}$ in Ref. [159]. Detector design is based on full-epitaxial p^{+}-p^{-}-n^{+} multilayer structures. The $5 \times 10^{12} cm^{-2}$ fluence is identified by the authors as a threshold: below it, SiC photodetectors maintain their performance, while above it, photosensitivity is reduced.

The effect of irradiation temperature on detector performance was studied by Ruddy et al. [98, 160]. They used a ^{238}Pu α source to test 4H-SiC detectors irradiated with fast neutrons at two temperatures, 45°C and 230°C. For both temperatures, CCE decreases linearly as a function of neutron fluence. This linearity suggests that the loss of charge carriers in the SiC active volume is proportional to the density of fast-neutron produced traps. The impact of temperature is significant. The authors discovered that SiC irradiated at 230 °C had a higher CCE (up to a factor of 2), indicating that high temperatures help CCE resist radiation damage, opening the possibility of using SiC neutron detectors in high-temperature environments. In Ref. [131], similar conclusions about the effects of temperature on radiation damage were found for electron and proton irradiation.

Finally, large area 4H-SiC Schottky diodes (up to 20 mm^2 area, with 50 μm epitaxial layer) equipped with a ^{6}LiF converter (about 100 μm thick) were tested as neutron detectors in an epithermal column devoted to Boron Neutron Capture Therapy (BNCT) applications in Ref. [161]. At neutron fluences in the $10^{9} - -10^{13} cm^{-2}$ range, which are typical for BNCT, α and ^{3}H emitted the $^{6}Li(n,\alpha)^{3}H$ reaction in the converter layer have been detected. After a fluence of $10^{13} n/cm^{2}$, counting rates remain stable, with only a slight decrease of 3%. This efficiency drop, according to the authors, is caused by defects produced by neutron-generated alpha particles.

6 Conclusion

This review describes the current state of SiC-based radiation detectors, as well as their performance.At the outset, the main material parameters that influence the performance of SiC detectors were summarized. Material growth, device construction, and characterization methods were briefly reviewed. Optimization studies on existing fabrication processes and the introduction of new ones during the last several years have resulted in the ability to produce high-quality SiC substrates and epitaxial layers on the one hand, and the ability to control the doping concentration of the latter on the other. These two objectives have resulted in high-quality SiC detectors that have been proved to be capable of detecting a wide range of radiations at various energies with good results.

In the future, two detector development directions should be explored. One is the ability to generate thicker (≥ 300 μm), higher-quality epitaxial layers with lower doping concentrations ($\leq 10^{12} cm^{-3}$). The major reason is that the detector must have a thick active region that can be drained with a fair amount of reverse bias. This is especially significant for detecting low-ionizing particles, increasing sensitivity to high-energy x-ray photons, improving direct rapid neutron detection, and decreasing detector capacitance, therefore increasing energy resolution. The other path of development is toward detectors with sub-micrometer thicknesses that can be employed for beam monitoring in synchrotron facilities of flash radiotherapy, for example.

The results achieved with existing SiC detectors and the consequences of high irradiation doses were discussed in the second part of the paper. For various types of radiations, some of the best results obtained thus far are reported. Based on these findings, it is obvious that current fabrication technology has matured to the point where SiC diodes capable of excellent performance when employed to detect various types of radiation are now possible.

SiC detectors have shown 100% CCE for ionizing radiation (electron, protons, alphas, and heavy ions) and energy resolutions that are usually only a few percent but can be as low as 0.5% percent in some optimized cases, putting SiC performance in terms of energy resolution not far behind standard Si detectors, with the advantage of SiC being able to operate at higher temperatures.

Irradiation of SiC detectors generally reveals that they are radiation-resistant. This is especially true for electron irradiation. Irradiation with protons and ions begins to degrade detector performance at fluences of $\sim 10^{15} p/cm^{2}$ and $\sim 2 \cdot 10^{14} ions/cm^{2}$, though these values are highly dependent on the detector structure and material starting quality. CCE loss can sometimes be compensated by over-biasing the detector.

SiC UV detector show high responsitivity in the ~ 250−350 nm range and are radiation resistance when irradiated with 1 MeV neutron up a fluence of $5 \times 10^{12} n/cm^{2}$.

X-ray sensitivity is up to ~ $60keV$, with a few percent energy resolution. With the added benefit of being able to function at high temperatures without losing performance.

In comparison to charged particles and fast neutrons, the effects of γ-rays on the operational lifetimes of SiC detectors are minor. Detector degradation begins at fluences greater than around 10^{14}–$10^{15} n/cm^{2}$ in the latter case.

SiC has begun to compete with diamonds in terms of energy resolution and sensitivity in fast neutron detection. In thermal neutron detection, an excellent degree of γ discrimination has been recorded, with ~ 100% sensitivity to neutrons.

All of the qualities found in SiC detectors make them intriguing devices for usage in a variety of domains, ranging from nuclear physics to astrophysics, *in vivo* dosimetry to beam monitoring, and monitoring hostile nuclear environments. SiC detectors have been employed for TOF measurements of high energy laser-driven beams and are proposed as diagnostic detector in flash radiotherapy. Furthermore, recent theoretical investigations have suggested that SiC could be useful for light DM detection.

The results obtained so far, and possible future improvements from further technological developments, make

the use of SiC detectors an exiting topic that will probably reserve, in the future, many other exiting outcomes in many application fields.

Author contributions

MD: author of the manuscript.

Acknowledgments

I would like to thank my son Ettore for having deeply inspired me in writing this paper. I will always remember with love the sleepless nights spent together.

Conflict of interest

The handling editor MM declared a shared committee Scientific Commitee 5 of the INFN with the author at the time of review.

Publisher's note

References

1. Berzelius J. Untersuchungen über die flussspathsäure und deren merkwürdigsten verbindungen. *Ann Phys Phys Chem* (1824) 1:169–230. doi:10.1002/andp.18240770603

2. Babcock R. Radiation damage in sic. *IEEE Trans Nucl Sci* (1965) 12:43–7. doi:10.1109/tns.1965.4323922

3. Kimoto T. *Fundamentals of silicon carbide technology: Growth, characterization, devices, and applications*. New York: John Wiley & Sons (2014).

4. Lindner JKN. *Silicon carbide: Recent major advances*. New York, NY, USA: Springer-Verlag B e r l i n Heidelberg (2004).

5. Nava F, Bertuccio G, Cavallini A, Vittone E. Silicon carbide and its use as a radiation detector material. *Meas Sci Technol* (2008) 19:102001. doi:10.1088/0957-0233/19/10/102001

6. Strokan N, Ivanov A, Lebedev A. *Silicon carbide nuclear- radiation detectors in SiC power materials: Devices and applications*. New York, NY, USA: Springer-Verlag (2009).

7. De Napoli M. *Silicon carbide radiation detectors*. New York: Nova Science Publishers (2011).

8. Ruddy FH. Silicon carbide radiation detectors: Progress, limitations and future directions. *Mater Res Soc Online Proc* (2013) 1576:101. doi:10.1557/opl.2013.1142

9. Capan I. 4h-sic Schottky barrier diodes as radiation detectors: A review. *Electronics* (2022) 11:532. doi:10.3390/electronics11040532

10. Zhao S, Gohil T, Lioliou G, Barnett A. Soft x-ray detection and photon counting spectroscopy with commercial 4h-sic Schottky photodiodes. *Nucl Instr Methods Phys Res Section A: Acc Spectrometers Detectors Associated Equipment* (2016) 830:1–5. doi:10.1016/j.nima.2016.05.053

11. Bertuccio G, Caccia S, Puglisi D, Macera D. Advances in silicon carbide x-ray detectors. *Nucl Instr Methods Phys Res Section A: Acc Spectrometers, Detectors Associated Equipment* (2011) 652:193–6. doi:10.1016/j.nima.2010.08.046

12. Strelchuk AM, Berenguier B, Yakimov EB, Ottaviani L. Recombination processes in 4h-sic pn structures. *Mater Sci Forum* (2007) 858:345–8. doi:10.4028/www.scientific.net/msf.858.345

13. De Napoli M, Giacoppo F, Raciti G, Rapisarda E. Study of charge collection efficiency in 4h–sic Schottky diodes with 12c ions. *Nucl Instr Methods Phys Res Section A: Acc Spectrometers, Detectors Associated Equipment* (2009) 608:80–5. doi:10.1016/j.nima.2009.06.018

14. Hiyoshi T, Kimoto T. Reduction of deep levels and improvement of carrier life-time in n-type 4h-sic by thermal oxidation. *Appl Phys Express* (2009) 2:041101. doi:10.1143/apex.2.041101

15. Løvlie LS, Svensson BG. Oxidation-enhanced annealing of implantation-induced Z1/2centers in 4H-SiC: Reaction kinetics and modeling. *Phys Rev B* (2012) 86:075205. doi:10.1103/physrevb.86.075205

16. Konstantinov AO, Wahab Q, Nordell N, Lindefelt U. Study of avalanche breakdown and impact ionization in 4h silicon carbide. *J Electron Mater* (1998) 27:335–41. doi:10.1007/s11664-998-0411-x

17. Kleppinger J, Chaudhuri S, Karadavut O, Mandal K. Defect characterization and charge transport measurements in high-resolution Ni/n-4H-SiC Schottky barrier radiation detectors fabricated on 250 μm epitaxial layers. *J Appl Phys* (2021) 129:244501. doi:10.1063/5.0049218

18. Ruddy FH, Dulloo AR, Seidel JG, Seshadri S, Rowland LB. Development of a silicon carbide radiation detector. *IEEE Trans Nucl Sci* (1998) 45:536–41. doi:10.1109/23.682444

19. Issa F, Vervisch V, Ottaviani L, Szalkai D, Vermeeren L, Lyoussi A, et al. Radiation silicon carbide detectors based on ion implantation of boron. *IEEE Trans Nucl Sci* (2004) 61:2105–11. doi:10.1109/tns.2014.2320943

20. Bozack MJ. Surface studies on sic as related to contacts. *Phys Status Solidi B* (2002) 549–80. doi:10.1002/1521-3951(199707)202:1¡549::AID-PSSB549¿3.0.CO;2-6

21. Crofton J, Porter LM, Williams JR. The physics of ohmic contacts in sic. *Phys Status Solidi B* (1997) 202:581–603. doi:10.1002/1521-3951(199707)202:1¡581::AID-PSSB581¿3.0.CO;2-M

22. Saxena V, Steckl A. Chapter 3 building blocks for SiC devices: Ohmic contacts, Schottky contacts, and p-n junctions. *Semiconductors and Semimetals* (1998) 52:77–160. doi:10.1016/S0080-8784(08)62845-8

23. Wagner G, Schulz D, Siche D. Vapour phase growth of epitaxial silicon carbide layers. *Prog Cryst Growth Characterization Mater* (2003) 47:139–65. doi:10.1016/j.pcrysgrow.2005.01.001

24. Wijesundara M, Azevedo R. *Silicon carbide microsystems for harsh enviroments*. New York, NY, USA: Springer (2011).

25. Glass R, Henshall D, Tsvetkov V, Carter C. Sic seeded crystal growth. *Phys Stat Sol* (1997) 202:149–62. doi:10.1002/1521-3951(199707)202:1<149::aid-pssb149>3.0.co;2-m

26. Straubinger TL, Wellmann P. Investigation of a pvt sic-growth set-up modified by an additional gas flow. *Mater Sci Forum* (2001) 353:33–6. doi:10.4028/www.scientific.net/MSF.353-356.33

27. Sun GL, Galben-Sandulache IG, Ouisse T, Dedulle JM, Pons M, Madar R, et al. Improvements of the continuous feed-physical vapor transport technique (cf-pvt) for the seeded growth of 3c-sic crystals. *Mater Sci Forum* (2010) 645-648:63–6. doi:10.4028/www.scientific.net/msf.645-648.63

28. Kordina O, Hallin C, Henry A, Bergman J, Ivanov I, Ellison A, et al. Growth of sic by hot-wall cvd and htcvd. *Phys Stat Sol* (1997) 202:321–34. doi:10.1002/1521-3951(199707)202:1<321::aid-pssb321>3.0.co;2-h

29. Cheng H, Yang M, Lai Y, Hu M, Li Q, Tu R, et al. Transparent highly oriented 3c-sic bulks by halide laser cvd. *J Eur Ceram Soc* (2018) 38:3057–63. doi:10.1016/j.jeurceramsoc.2018.03.015

30. Ujihara T, Seki K, Tanaka R, Kozawa S, Morimoto K, Sasaki K, et al. High-quality and large-area 3c–sic growth on 6h–sic(0 0 0 1) seed crystal with top-seeded solution method. *J Cryst Growth* (2011) 318:389–93. doi:10.1016/j.jcrysgro.2010.10.148

31. Kusunoki K, Kamei K, Okada N, Moriguchi K, Kaido H, Daikoku H, et al. Top-seeded solution of 3 inch diameter 4h-sic bulk crystal using metal solvents. *Mater Sci Forum* (2014) 49:778–80. doi:10.4028/www.scientific.net/MSF.778-780.79

32. Kordina O, Hallin C, Ellison A, Bakin AS, Ivanov IG, Henry A, et al. High temperature chemical vapor deposition of sic. *Appl Phys Lett* (1996) 69:1456–8. doi:10.1063/1.117613

33. Yakimova R, Janzn E. Current status and advances in the growth of sic. *Diamond Relat Mater* (2000) 9:432–8. doi:10.1016/s0925-9635(99)00219-8

34. Ferro G, Chaussende D, Jacquier C. VLS growth of SiC epilayers. M. Syväjârvi and R. Yakimova. Wide band gap materials and new developments.. *Research signpost* (2006) 91–116. hal-00140374.

35. Kern R, Jarrendahl K, Tanaka S, Davis R. Homoepitaxial sic growth by molecular beam epitaxy. *Phys Stat Sol* (1997) 202:379–404. doi:10.1002/1521-3951(199707)202:1<379::aid-pssb379>3.0.co;2-2

36. Dahal R, Chowdhury S, Hitchcock CW, Chow TP, Bhat IB. Fabrication of thick free-standing lightly-doped n-type 4h-sic wafers. *Mater Sci Forum* (2017) 897: 379–82. doi:10.4028/www.scientific.net/msf.897.379

37. Nida S, Tsibizov A, Ziemann T, Woerle J, Moesch A, Schulze-Briese C, et al. Silicon carbide x-ray beam position monitors for synchrotron applications. *J Synchrotron Radiat* (2019) 26:28–35. doi:10.1107/S1600577518014248

38. Henry CH, Lang DV. Nonradiative capture and recombination by multi-phonon emission in gaas and gap. *Phys Rev B* (1977) 15:989–1016. doi:10.1103/physrevb.15.989

39. Peaker AR, Markevich VP, Coutinho J. Tutorial: Junction spectroscopy techniques and deep-level defects in semiconductors. *J Appl Phys* (2018) 123: 161559. doi:10.1063/1.5011327

40. Wahab Q, Ellison A, Henry A, Janzén E, Hallin C, Di Persio J, et al. Influence of epitaxial growth and substrate-induced defects on the breakdown of 4H–SiC Schottky diodes. *Appl Phys Lett* (2000) 76:2725–7. doi:10.1063/1.126456

41. Izumi S, Tsuchida H, Tawara T, Kamata I, Izumi K. Structure of in-grown stacking faults in the 4h–sic epitaxial layers. *Mater Sci Forum* (2005) 483-485:323–6. doi:10.4028/www.scientific.net/msf.483-485.323

42. Fujiwara H, Kimoto T, Tojo T, Matsunami H. Reduction of stacking faults in fast epitaxial growth of 4H-SiC and its impacts on high-voltage Schottky diodes. *Mater Sci Forum* (2005) 483-485:151–4. doi:10.4028/www.scientific.net/msf.483-485.151

43. Choyke WJ, Matsunami H, Pensl G. *Silicon carbide: Recent major advances, advanced texts in physics*. Berlin: Springer-Verlag (2004).

44. Kimoto T, Cooper JA. *Fundamentals of silicon carbide technology: Growth, characterization, devices, and applications*. Singapore: John Wiley & Sons (2014).

45. Capan I, Brodar T, Coutinho J, Ohshima T, Markevich V, Peaker A. Acceptor levels of the carbon vacancy in 4*h*-sic: Combining laplace deep level transient spectroscopy with density functional modeling. *J Appl Phys* (2018) 124:245701. doi:10.1063/1.5063773

46. Pastuović Z, Siegele R, Capan I, Brodar I, Sato S, Ohshima T. Deep level defects in 4h-sic introduced by ion implantation: The role of single ion regime. *J Phys : Condens Matter* (2017) 29:475701. doi:10.1088/1361-648x/aa908c

47. Ayedh HM, Hallén A, Svensson BG. Elimination of carbon vacancies in 4h-sic epi-layers by near-surface ion implantation: Influence of the ion species. *J Appl Phys* (2015) 118:175701. doi:10.1063/1.4934947

48. Ayedh HM, Nipoti R, Hallén A, Svensson BG. Thermodynamic equili- bration of the carbon vacancy in 4h-sic: A lifetime limiting defect. *J Appl Phys* (2017) 122: 025701. doi:10.1063/1.4991815

49. Storasta L, Tsuchida H. Reduction of traps and improvement of carrier lifetime in 4h-sic epilayers by ion implantation. *Appl Phys Lett* (2007) 90:062116. doi:10.1063/1.2472530

50. Miyazawa T, Tsuchida H. Point defect reduction and carrier lifetime improvement of si- and c-face 4h-sic epilayers. *J Appl Phys* (2013) 113:083714. doi:10.1063/1.4793504

51. Ayedh HM, Nipoti R, Hallén A, Svensson BG. Elimination of carbon vacancies in 4h-sic employing thermodynamic equilibrium conditions at moderate temperatures. *Appl Phys Lett* (2013) 107:252102. doi:10.1063/1.4938242

52. Okamoto K, Kikuchi T, Ikeda A, Ikenoue H, Asano T. Formation of low resistance contacts to p-type 4H-SiC using laser doping with an Al thin-film dopant source. *Jpn J Appl Phys* (2019) 58:SDDF13. doi:10.7567/1347-4065/ab12c3

53. Zhou Z, He W, Zhang Z, Sun J, Schöner A, Zheng Z. Characteristics of ni-based ohmic contacts on n-type 4h-sic using different annealing methods. *Nanotechnol Precis Eng* (2021) 4:013006. doi:10.1063/10.0003763

54. Shalish I, Shapira Y. Thermal stability of Re Schottky contacts to 6H-SiC. *IEEE Electron Device Lett* (2000) 21:581–3. doi:10.1109/55.887472

55. Teraji T, Hara S, Okushi H, Kajimura K. Ideal ohmic contact to n-type 6h–sic by reduction of Schottky barrier height. *Appl Phys Lett* (1997) 71:689–91. doi:10.1063/1.119831

56. Nava F, Wagner G, Lanzieri C, Vanni P, Vittone E. Investigation of ni/4h–sic diodes as radiation detectors with low doped n-type 4h–sic epilayers. *Nucl Instr Methods Phys Res Section A: Acc Spectrometers Detectors Associated Equipment* (2003) 510:273–80. doi:10.1016/S0168-9002(03)01868-0

57. Kumta A, Rusli, Xia JH. Passivation of 4h–sic Schottky barrier diodes using aluminum based dielectrics. *Solid-State Electronics* (2000) 53:204–10. doi:10.1016/j.sse.2008.11.004

58. De Napoli M, Giacoppo F, Raciti G, Rapisarda E. Dopant concentration dependence of the response of sic Schottky diodes to light ions. *Nucl Instr Methods Phys Res Section A: Acc Spectrometers, Detectors Associated Equipment* (2009) 600: 618–23. doi:10.1016/j.nima.2008.12.109

59. Moscatelli F, Scorzoni A, Poggi A, Bruzzi M, Sciortino S, Lagomarsino S, et al. Radiation hardness after very high neutron irradiation of minimum ionizing particle detectors based on 4H-SiC p/sup +/n junctions. *IEEE Trans Nucl Sci* (2006) 53:1557–63. doi:10.1109/TNS.2006.872202

60. Nava F, Vanni P, Bruzzi M, Lagomarsino S, Sciortino S, Wagner G, et al. Minimum ionizing and alpha particles detectors based on epitaxial semiconductor silicon carbide. *IEEE Trans Nucl Sci* (2004) 51:238–44. doi:10.1109/TNS.2004.825095

61. Rogalla M, Runge K, Söldner-Rembold A. Particle detectors based on semi-insulating silicon carbide. *Nucl Phys B - Proc Supplements* (1999) 78:516–20. doi:10.1016/S0920-5632(99)00596-4

62. Bruzzi M, Lagomarsino S, Nava F, Sciortino S. Characterisation of epitaxial sic Schottky barriers as particle detectors. *Diamond Relat Mater* (2003) 12:1205–8. doi:10.1016/S0925-9635(02)00350-3

63. Lo Giudice A, Fizzotti F, Manfredotti C, Vittone E, Nava F. Average energy dissipated by mega-electron-volt hydrogen and helium ions per electron-hole pair generation in 4H-SiC. *Appl Phys Lett* (2005) 87:222105. doi:10.1063/1.2135507

64. De Napoli M, Raciti G, Rapisarda E, Sfienti C. Light ions response of silicon carbide detectors. *Nucl Instr Methods Phys Res Section A: Acc Spectrometers, Detectors Associated Equipment* (2007) 572:831–8. doi:10.1016/j.nima.2006.12.039

65. Bernat R, Capan I, Bakra ōc L, Brodar T, Makino T, Ohshima T, et al. Response of 4h-sic detectors to ionizing particles. *Crystals* (2021) 11:10. doi:10.3390/cryst11010010

66. Zatko B, Dubecký F, Šagátová A, Sedlačová K, Ryć L. High resolution alpha particle detectors based on 4h-sic epitaxial layer. *J Instrumentation* (2015) 10: C04009. doi:10.1088/1748-0221/10/04/C04009/pdf

67. Chaudhuri SK, Karadavut O, Kleppinger JW, Mandala KC. High-resolution radiation detection using ni/sio2/n-4h-sic vertical metal-oxide-semiconductor capacitor. *J Appl Phys* (2021) 130:074501. doi:10.1063/5.0059151

68. Ruddy F, Seidel J, Chen H, Dulloo A, Ryu S. High-resolution alpha-particle spectrometry using 4h silicon carbide semiconductor detectors. *IEEE Trans Nucl Sci* (2006) 53:1713–8. doi:10.1109/tns.2006.875155

69. Ivanov AM, Kalinina EV, Kholuyanov G, Strokan NB, Onushkin G, Konstantinov AO, et al. High energy resolution detectors based on 4h–sic. *Mater Sci Forum* (2005) 483:4851029–32. doi:10.4028/www.scientific.net/msf.483-485.1029

70. Chaudhuri SK, Zavalla KJ, Mandal KC. High resolution alpha particle detection using 4h–sic epitaxial layers: Fabrication, characterization, and noise analysis. *Nucl Instr Methods Phys Res Section A: Acc Spectrometers, Detectors Associated Equipment* (2013) 728:97–101. doi:10.1016/j.nima.2013.06.076

71. Zatko B, Hrubčín L, Šagátová A, Osvald J, Boháček P, Kováčová E, et al. Study of Schottky barrier detectors based on a high quality 4h-sic epitaxial layer with different thickness. *Appl Surf Sci* (2021) 536:147801. doi:10.1016/j.apsusc.2020.147801

72. Zhang X, Cates JW, Hayward JP, Bertucio G, Pulglisi D, Hausladen PA. Characterizing the timing performance of a fast 4h-sic. *IEEE Trans Nucl Sci* (2013) 60:2352–6. doi:10.1109/TNS.2013.2260652

73. Breese M. A theory of ion beam induced charge collection. *J Appl Phys* (1993) 74:3789–99. doi:10.1063/1.354471

74. Milluzzo G, Scuderi V, Amico A, Borghesi M, Cirrone G, Cuttone G, et al. Laser-accelerated ion beam diagnostics with tof detectors for the elimed beam line. *J Instrum* (2017) 12:C02025. doi:10.1088/1748-0221/12/02/C02025

75. Bertuccio G, Puglisi D, Torrisi L, Lanzieri C. Silicon carbide detector for laser-generated plasma radiation. *Appl Surf Sci* (2013) 272:128–31. doi:10.1016/j.apsusc.2012.03.183

76. Brown D, Downey E, Ghezzo M, Kretchmer J, Saia R, Liu Y, et al. Silicon carbide UV photodiodes. *IEEE Trans Electron Devices* (1993) 40:325–33. doi:10.1109/16.182509

77. Sciuto A, Mazzillo M, Franco SD, Roccaforte F, D'Arrigo G. Visible blind 4h-sic p $^{+}$-n uv photodiode obtained by al implantation. *IEEE Photon J* (2015) 7:1–6. doi:10.1109/JPHOT.2015.2439955

78. Yan F, Xin X, Aslam S, Zhao Y, Franz D, Zhao J, et al. 4h–sic photodiodes detectors with large area and very high specific detectivity. *IEEE Quan Electron* (2004) 40:1315. doi:10.1109/JQE.2004.833196

79. Sciuto A, Roccaforte F, Franco SD, Raineri V, Bonanno G. High responsivity 4H-SiC Schottky UV photodiodes based on the pinch-off surface effect. *Appl Phys Lett* (2006) 89:081111. doi:10.1063/1.2337861

80. Ng B, David J, Tozer R, Rees G, Feng Y, Zhao J, et al. Nonlocal effects in thin 4h–sic uv avalanche photodiodes. *IEEE Trans Electron Devices* (2003) 50:1724–32. doi:10.1109/TED.2003.815144

81. Yan F, Qin C, Zhao J, Bush M, Olsen G, Ng B, et al. Demonstration of 4h–sic avalanche photodiodes linear array. *Solid State Electron* (2003) 47:241–5. doi:10.1016/S0038-1101(02)00201-0

82. Bertuccio G, Casiraghi R, Nava F. Epitaxial silicon carbide for x-ray detection. *IEEE Trans Nucl Sci* (2001) 48:232–3. doi:10.1109/23.915369

83. Lees J, Bassford D, Fraser G, Horsfall A, Vassilevski K, Wright N, et al. Semi-transparent sic Schottky diodes for x-ray spectroscopy. *Nucl Instr Methods Phys Res Section A: Acc Spectrometers Detectors Associated Equipment* (2007) 578:226–34. doi:10.1016/j.nima.2007.05.172

84. Mandal KC, Muzykov PG, Terry JR. Highly sensitive x-ray detectors in the low-energy range on n-type 4H-SiC epitaxial layers. *Appl Phys Lett* (2012) 101: 051111. doi:10.1063/1.4742741

85. Mandal KC, Chaudhuri SK, Nguyen K. An overview of application of 4h- sic n-type epitaxial Schottky barrier detector for high resolution nuclear detec- tion. IEEE Nuclear Science Symposium and Medical Imaging Confer- ence (2013 NSS/MIC)(2013). doi:10.1109/nssmic.2013.6829844

86. Lioliou G, Chan HK, Gohil T, Vassilevski KV, Wright NG, Horsfall AB, et al. 4h-sic Schottky diode arrays for x-ray detection. *Nucl Instr Methods Phys Res Section A: Acc Spectrometers Detectors Associated Equipment* (2016) 840:145–52. doi:10.1016/j.nima.2016.10.002

87. Lioliou G, Gemmell NR, Mazzillo M, Sciuto A, Barnett AM. 4H-SiC Schottky diodes with Ni2Si contacts for X-ray detection. *Nucl Instr Methods Phys Res Section A: Acc Spectrometers Detectors Associated Equipment* (2019) 940:328–36. doi:10.1016/j.nima.2019.06.036

88. Puglisi D, Bertuccio G. Silicon carbide microstrip radiation detectors. *Micromachines (Basel)* (2019) 10:835. doi:10.3390/mi10120835

89. Bruzzi M, Nava F, Russo S, Sciortino S, Vanni P. Characterisation of silicon carbide detectors response to electron and photon irradiation. *Diamond Relat Mater* (2001) 10:657–61. doi:10.1016/S0925-9635(00)00380-0

90. Bertuccio G, Puglisi D, Macera D, Liberto RD, Lamborizio M, Mantovani L. Silicon carbide detectors for in vivo dosimetry. *IEEE Trans Nucl Sci* (2014) 61: 961–6. doi:10.1109/TNS.2014.2307957

91. Rafi JM, Pellegrini G, Godignon P, Ugobono SO, Rius G, Tsunoda I, et al. Electron, neutron, and proton irradiation effects on sic radiation detectors. *IEEE Trans Nucl Sci* (2020) 67:2481–9. doi:10.1109/TNS.2020.3029730

92. Marinelli M, Milani E, Prestopino G, Tucciarone A, Verona C, Verona-Rinati G, et al. Synthetic single crystal diamond as a fission reactor neutron flux monitor. *Appl Phys Lett* (2007) 90:183509. doi:10.1063/1.2734921

93. Angelone M, Lattanzi D, Pillon M, Marinelli M, Milani E, Tucciarone A, et al. Development of single crystal diamond neutron detectors and test at jet tokamak. *Nucl Instr Methods Phys Res Section A: Acc Spectrometers, Detectors Associated Equipment* (2008) 595:616–22. doi:10.1016/j.nima.2008.07.107

94. Almaviva S, Marinelli M, Milani E, Prestopino G, Tucciarone A, Verona C, et al. Thermal and fast neutron detection in chemical vapor deposition single-crystal diamond detectors. *J Appl Phys* (2008) 103:054501. doi:10.1063/1.2838208

95. Pompili F, Esposito B, Marocco D, Podda S, Riva M, Baccaro S, et al. Radiation and thermal stress test on diamond detectors for the radial neutron camera of iter. *Nucl Instr Methods Phys Res Section A: Acc Spectrometers, Detectors Associated Equipment* (2019) 936:62–4. doi:10.1016/j.nima.2018.10.110

96. Franceschini F, Ruddy FH. *Silicon carbide neutron detectors*. Rijeka, Croatia: Properties and Applications of Silicon Carbide (2011). p. 275–96.

97. Coutinho J, JBTorres V, Capan I, Brodar T, Ereš Z, Bernat R, et al. Silicon carbide diodes for neutron detection. *Nucl Instr Methods Phys Res Section A: Acc Spectrometers, Detectors Associated Equipment* (2021) 986:164793. doi:10.1016/j.nima.2020.164793

98. Ruddy FH, Ottaviani L, Lyoussi A, Destouches C, Palais O, Carette CR. Performance and applications of silicon carbide neutron detectors in harsh nuclear environments. *EPJ Web Conf* (2021) 253:11003. doi:10.1051/epjconf/202125311003

99. Dulloo A, Ruddy F, Seidel J, Adams J, Nico J, Gilliam DM. The neutron response of miniature silicon carbide semiconductor detectors. *Nucl Instr Methods Phys Res Section A: Acc Spectrometers, Detectors Associated Equipment* (1999) 422: 47–8. doi:10.1016/s0168-9002(98)01060-2

100. Dulloo A, Ruddy F, Seidel J, Adams J, Nico J, Gilliam DM. The thermal neutron response of miniature silicon carbide semiconductor detectors. *Nucl Instr Methods Phys Res Section A: Acc Spectrometers, Detectors Associated Equipment* (2003) 498:415–23. doi:10.1016/s0168-9002(02)01987-3

101. Dulloo A, Ruddy F, Seidel J, Davison C, Flinchbaugh T, Daubenspeck T. Simultaneous measurement of neutron and gamma-ray radiation levels from a triga reactor core using silicon carbide semiconductor detectors. *IEEE Trans Nucl Sci* (1999) 46:275–9. doi:10.1109/23.775527

102. Dulloo AR, Ruddy FH, Seidel JG, Flinchbaugh T, Davison C. Neutron and gamma ray dosimetry in spent- fuel radiation environments using silicon carbide semiconductor radiation detectors. In: JG Williams, DW Vehar, FH Ruddy, DM Gilliam, editors. *Reactor dosimetry: Radiation metrology and assessment, ASTM STP 1398* (2001). p. 683–90.

103. Ruddy FH, Seidel JG, Blue TE, Miller DW. *Reactor power monitoring using silicon carbide fast neutron detectors*. La Grange Park, IL, United States: web. PHYSOR-2006 – American Nuclear Society's Topical Meeting on Reactor Physics (2006).

104. Obraztsova O, Ottaviani L, Klix A, Doring T, Palais O, Lyoussi A. Comparing the response of a SiC and a sCVD diamond detectors to 14-MeV neutron radiation. *IEEE Trans Nucl Sci* (2018) 65:2380–4. doi:10.1109/tns.2018.2848469

105. Szalkai D, Ferone R, Issa F, Klix A, Lazar M, Lyoussi A, et al. Fast neutron detection with 4h-sic based diode detector up to 500 °c ambient temperature. *IEEE Trans Nucl Sci* (2016) 63:1491–8. doi:10.1109/tns.2016.2522921

106. Obraztsova O, Ottaviani L, Geslot B, de Izarra G, Palais O, Lyoussi A, et al. Comparison between silicon carbide and diamond for thermal neutron detection at room temperature. *IEEE Trans Nucl Sci* (2020) 67:863–71. doi:10.1109/tns.2020.2981059

107. Flammang RW, Seidel JG, Ruddy FH. Fast neutron detection with silicon carbide semiconductor radiation detectors. *Nucl Instr Methods Phys Res Section A: Acc Spectrometers, Detectors Associated Equipment* (2007) 579:177–9. doi:10.1016/j.nima.2007.04.034

108. Wu J, Jiang Y, Li M, Zeng L, Li J, Gao H, et al. Development of high sensitivity 4h–sic detectors for fission neutron pulse shape measurements. *Rev Scientific Instr* (2017) 88:083301. doi:10.1063/1.4995811

109. Hodgson M, Lohstroh A, Sellin P, Thomas D. Characterization of silicon carbide and diamond detectors for neutron applications. *Meas Sci Technol* (2017) 28:105501. doi:10.1088/1361-6501/aa7f8b

110. Hodgson M, Lohstroh A, Sellin P, Thomas D. Neutron detection performance of silicon carbide and diamond detectors with incomplete charge collection properties. *Nucl Instr Methods Phys Res Section A: Acc Spectrometers, Detectors Associated Equipment* (2017) 847:1–9. doi:10.1016/j.nima.2016.11.006

111. Angelone M, Cesaroni S, Loreti S, Pagano G, Pillon M. High temperature response of a single crystal CVD diamond detector operated in current mode. *Nucl Instr Methods Phys Res Section A: Acc Spectrometers Detectors Associated Equipment* (2019) 943:162493. doi:10.1016/j.nima.2019.162493

112. Mandal KC, Chowdhury TA, Oner C, Ruddy FH. *Design and response testing of boron-diffused silicon carbide neutron detectors for dosimetry and monitoring applications*. PA, USA (2018). Available at: https://www.astm.org/stp160820170042.html.

113. Issa F, Ottaviani L, Szalkai D, Vermeeren L, Vervisch V, Lyoussi A, et al. Improvements in realizing 4h-sic thermal neutron detectors. *EPJ Web of Conferences* (2016) 106:05004. doi:10.1051/epjconf/201610605004

114. Radulovic V, Yamazaki Y, Pastuovic Z, Sarbutt A, Ambrožic õ K, Bernat R, et al. Silicon carbide neutron detector testing at the jsi triga reactor for enhanced border and port security. *Nucl Instr Methods Phys Res Section A: Acc Spectrometers, Detectors Associated Equipment* (2020) 972:164122. doi:10.1016/j.nima.2020.164122

115. Scuderi V, Milluzzo G, Alejo A, Amico A, Booth N, Cirrone G, et al. Time of flight based diagnostics for high energy laser driven ion beams. *J Instrum* (2017) 12: C03086. doi:10.1088/1748-0221/12/03/C03086

116. Margarone D, Krása J, Giuffrida L, Picciotto A, Torrisi L, Nowak T, et al. Full characterization of laser-accelerated ion beams using faraday cup, silicon carbide, and single-crystal diamond detectors. *J Appl Phys* (2011) 109:103302. doi:10.1063/1.3585871

117. Romano F, Del Mar Carulla Areste M, Camarda M. Feasibility study of using innovative technology based on silicon carbide detectors for flash irradiations. *Phys Med* (2022) 94:S97–8. doi:10.1016/s1120-1797(22)01662-3

118. Griffin SM, Hochberg Y, Inzani K, Kurinsky N, Lin T, Yu TC. Silicon carbide detectors for sub-gev dark matter. *Phys Rev D* (2021) 103:075002. doi:10.1103/PhysRevD.103.075002

119. Bathen M, Galeckas A, Müting J, Ayedh H, Grossner U, Coutinho J, et al. Electrical charge state identification and control for the silicon vacancy in 4h-sic. *NPJ Quan Inf* (2019) 5:111. doi:10.1038/s41534-019-0227-y

120. Alfieri G, Mihaila A. Isothermal annealing study of the eh1 and eh3 levels in n-type 4h-sic. *J Phys : Condens Matter* (2020) 32:465703. doi:10.1088/1361-648x/abaeaf

121. Karsthof R, Bathen M, Galeckas A, Vines L. Conversion pathways of primary defects by annealing in proton-irradiated n-type 4H-SiC. *Phys Rev B* (2020) 102: 184111. doi:10.1103/physrevb.102.184111

122. Nava F, Vittone E, Vanni P, Verzellesi G, Fuochi P, Lanzieri C, et al. Radiation tolerance of epitaxial silicon carbide detectors for electrons, protons and gamma-rays. *Nucl Instr Methods Phys Res Section A: Acc Spectrometers, Detectors Associated Equipment* (2003) A505:645–55. doi:10.1016/s0168-9002(02)01558-9

123. Ohyama H, Takakura K, Watanabe T, Nishiyama K, Shigaki K, Kudou T, et al. Radiation damage of sic Schottky diodes by electron irradiation. *J Mater Sci Mater Electron* (2005) 16:455–8. doi:10.1007/s10854-005-2314-4

124. Kang S, Ha J, Park S, Kim H, Chun S, Kim Y. Study of the current-voltage characteristics of a sic radiation detector irradiated by co-60 gamma-rays. *Nucl Instr Methods Phys Res Section A: Acc Spectrometers, Detectors Associated Equipment* (2007) A579:145–7. doi:10.1016/j.nima.2007.04.025

125. Ruddy F, Seidel J. The effects of intense gamma-irradiation on the alpha-particle response of silicon carbide semiconductor radiation detectors. *Nucl Instr Methods Phys Res Section B: Beam Interactions Mater Atoms* (2007) B263:163–8. doi:10.1016/j.nimb.2007.04.077

126. Liu L, Liu A, Bai S, Lv L, Jin P, Ouyang X. Radiation resistance of silicon carbide Schottky diode detectors in d-t fusion neutron detection. *Sci Rep* (2017) 7: 13376. doi:10.1038/s41598-017-13715-3

127. Sciortino S, Hartjes F, Lagomarsino S, Nava F, Brianzi M, Cindro V, et al. Effect of heavy proton and neutron irradiations on epitaxial 4h-sic Schottky diodes. *Nucl Instr Methods Phys Res Section A: Acc Spectrometers, Detectors Associated Equipment* (2005) 552:138–45. doi:10.1016/j.nima.2005.06.017

128. Wu J, Jiang Y, Lei J, Fan X, Chen Y, Li M, et al. Effect of neutron irradiation on charge collection efficiency in 4h-sic Schottky diode. *Nucl Instr Methods Phys Res Section A: Acc Spectrometers, Detectors Associated Equipment* (2014) 735:218–22. doi:10.1016/j.nima.2013.09.041

129. Liu L, Li F, Bai S, Jin P, Cao X, Ouyang X. Silicon carbide pin diode detectors used in harsh neutron irradiation. *Sensors Actuators A: Phys* (2018) 280:245–51. doi:10.1016/j.sna.2018.07.053

130. Liu L, Ouyang X, Ruan JL, Bai S, Ouyang XP. Performance comparison between sic and si neutron detectors in deuterium-tritium fusion neutron irradiation. *IEEE Trans Nucl Sci* (2019) 66:737–41. doi:10.1109/TNS.2019.2901797

131. Lebedev AA, Kozlovski VV, Davydovskaya KS, Levinshtein ME. Radiation hardness of silicon carbide upon high-temperature electron and proton irradiation. *Materials (Basel)* (2021) 14:4976. doi:10.3390/ma14174976

132. Ivanov AM, Strokan NB, Davydov DV, Savkina NS, Lebedev AA, Mironov YT, et al. Radiation hardness of sic ion detectors under relativistic protons. *Semiconductors* (2001) 35:481–4. doi:10.1134/1.1365200

133. Lebedev AA, Veinger AI, Davydov DV, Kozlovski VV, Savkina NS, Strel'chuk AM. Doping of n-type 6h–sic and 4h–sic with defects created with a proton beam. *J Appl Phys* (2000) 88:6265–71. doi:10.1063/1.1309055

134. Lebedev AA, Ivanov AM, Strokan NB. Radiation resistance of sic and nuclear radiation detectors based on sic films. *Semiconductors* (2004) 38:125–50. doi:10.1134/1.1648363

135. Castaldini A, Cavallini A, Rigutti L, Nava F, Ferrero S, Giorgis F. Deep levels by proton and electron irradiation in 4H–SiC. *J Appl Phys* (2005) 98:053706. doi:10.1063/1.2014941

136. Nava F, Vittone E, Vanni P, Fuochi P, Lanzieri C. Radiation tolerance of epitaxial silicon carbide detectors for electrons and -rays. *Nucl Instr Methods Phys Res Section A: Acc Spectrometers, Detectors Associated Equipment* (2003) 514: 126–34. doi:10.1016/j.nima.2003.08.094

137. Danno K, Kimoto T. Investigation of deep levels in n -type 4h-sic epilayers irradiated with low-energy electrons. *J Appl Phys* (2006) 100:113728. doi:10.1063/1.2401658

138. Kozlovskii V, Bogdanova E, Emtsev V, Emtsev K, Lebedev A, Lomasov V. Direct experimental comparisson of the effects of electron irradiation on the charge carrier removal rate in n-type silicon and silicon carbide. *Mater Sci Forum* (2004) 483–485:385–8. doi:10.4028/www.scientific.net/MSF.483

139. Kozlovski V, Lebedev A, Lomasov V, Bogdanova E, Seredova N. Conductivity compensation in n-4h-sic (cvd) under irradiation with 0.9-mev electrons. *Semiconductors* (2014) 48:1006–9. doi:10.1134/s1063782614080156

140. Strelchuk A, Kozlovskii V, Lebedev A, Smirnova N. Influence of irradiation on exess currents in sic pn structures. *Mater Sci Forum* (2004) 483-485:1001–4. doi:10.3390/ma14174976

141. Mikelsen M, Grossner U, Bleka J, Monakhov E, Swensson B, Yakimova R, et al. Carrier removal rate in electron irradiated 4h and 6h sic. *Mater Sci Forum* (2009) 600:425–8. doi:10.4028/www.scientific.net/MSF.600-603.425

142. Omotoso E, Meyer W, Auret F, Paradzah A, Diale M, Coelho S, et al. The influence of high energy electron irradiation on the Schottky barrier height and the richardson constant of ni/4h-sic Schottky diodes. *Mater Sci Semicond Process* (2015) 39:112–8. doi:10.1016/j.mssp.2015.04.031

143. Kozlovski V, Lebedev A, Levinshtein M, Rumyantsev S, Palmour J. Impact of high energy electron irradiation on high voltage ni/4h-sic Schottky diodes. *Appl Phys Lett* (2017) 110:083503. doi:10.1063/1.4977095

144. Balandovich VS. Deep-level transient spectroscopy of radiation-induced levels in 6h–sic. *Semiconductors* (1999) 33:1188–92. doi:10.1134/1.1187846

145. Gong M, Fung S, Beling C, You Z. A deep level transient spectroscopy study of electron irradiation induced deep levels in p-type 6h-sic. *J Appl Phys* (1999) 85: 7120–2. doi:10.1063/1.370520

146. Doyle J, Aboelfotoh M, Svensson B, Schöner A, Nordell N. Characterization of electrically active deep level defects in 4H and 6H SiC. *Diam Relat Mater* (1997) 6: 1388–91. doi:10.1016/S0925-9635(97)00102-7

147. Hemmingsson C, Son N, Kordina O, Bergman J, Janzén E, Lindstrom JL, et al. Deep level defects in electron-irradiated 4H SiC epitaxial layers. *J Appl Phys* (1997) 81:6155–9. doi:10.1063/1.364397

148. Castaldini A, Cavallini A, Rigutti L, Nava F. Electronic levels introduced by irradiation in silicon carbide. *Mater Sci Forum* (2002) 359:483–5. doi:10.4028/www.scientific.net/MSF.483-485.359

149. Sciuto A, Calcagno L, Franco SD, Pellegrino D, Selgi LM, D'Arrigo G. Radiation hardness of 4h-sic p-n junction uv photo-detector. *Materials* (2022) 15: 264. doi:10.3390/ma15010264

150. Kamezawa C, Sindou H, Hirao T, Ohyama H, Kuboyama S. Heavy ion-induced damage in sic Schottky barrier diode. *Physica B: Condensed Matter* (2008) 376:377362–6. doi:10.1016/j.physb.2005.12.093

151. Klanner R, Fretwurst E, Pintilie I, Schwandt J, Zhang J. Study of high-dose x-ray radiation damage of silicon sensors. *Nucl Instr Methods Phys Res Section A: Acc Spectrometers, Detectors Associated Equipment* (2013) 732:117–21. doi:10.1016/j.nima.2013.05.131

152. Ruddy F, Siedel J. Effects of gamma irradiation on silicon carbide semiconductor radiation det ectors. *Nucl Sci Symp Conf Rec* (2006) 1:583. doi:10.1109/NSSMIC.2006.356223

153. Park J, Park S, Shin H, Kim H, Kim J, Lee S, et al. Effect of metal electrode on characteristics of gamma-irradiated silicon carbide detector. *J Nucl Sci Technology* (2014) 51:482–6. doi:10.1080/00223131.2014.875956

154. Metzger S, Henschel H, Kohn O, Lennartz W. Silicon carbide radiation detector for harsh environments. *IEEE Trans Nucl Sci* (2002) 49:1351–5. doi:10.1109/tns.2002.1039666

155. Kinoshita A, Iwami M, Kobayashi K, Nakano I, Tanaka R, Kamiya T, et al. Radiation effect on pn-sic diode as a detector. *Nucl Instr Methods Phys Res Section A: Acc Spectrometers, Detectors Associated Equipment* (2005) 541:213–20. doi:10.1016/j.nima.2005.01.059

156. Brodar T, Capan I, Radulovic V, Snoj L, Pastuovic Z, Coutinho J, et al. Laplace DLTS study of deep defects created in neutron-irradiated n-type 4H-SiC. *Nucl Instr Methods Phys Res Section B: Beam Interactions Mater Atoms* (2018) 437: 27–31. doi:10.1016/j.nimb.2018.10.030

157. Seshadri S, Dulloo A, Ruddy F, Seidel JG, Rowland LB. Demonstration of an SiC neutron detector for high-radiation environments. *IEEE Trans Electron Devices* (1999) 46:567–71. doi:10.1109/16.748878

158. Nava F, Castaldini A, Cavallini A, Errani P, Cindro V. Radiation detection properties of 4H-SiC Schottky diodes irradiated up to10^16n/cm$2$by 1 MeV neutrons. *IEEE Trans Nucl Sci* (2006) 53:2977–82. doi:10.1109/tns.2006.882777

159. Afanasyev AV, Ilyin VA, Luchinin VV, Reshanov SA, Schöner A, Sergushichev K, et al. Effect of neutron irradiation on epitaxial 4h-sic pin uv-photodiodes. *Mater Sci Forum* (2017) 897:614–7. doi:10.4028/www.scientific.net/msf.897.614

160. Ruddy FH, Dulloo AR, Seidel JG. Study of the radiation resistance of silicon carbide radiation detectors. *Trans Am Nucl Soc* (2004) 90:348–9. doi:10.1016/j.nima.2013.09.041

161. Giudice AL, Fasolo F, Durisi E, Manfredotti C, Vittone E, Fizzotti F, et al. Performances of 4h-sic Schottky diodes as neutron detectors. *Nucl Instr Methods Phys Res Section A: Acc Spectrometers Detectors Associated Equipment* (2007) 583: 177–80. doi:10.1016/j.nima.2007.08.241